MAY 2017 M.Sc. in Electrical and Electronics Engineering SALAH HAFFAR

UNIVERSITY OF GAZİANTEP
GRADUATE SCHOOL OF
NATURAL & APPLIED SCIENCES

DETERMINATION OF OPTICAL CONSTANTS BY USING THZ TIME-DOMAIN SPECTROSCOPY

M.Sc. THESIS
IN
ELECTRICAL AND ELECTRONICS ENGINEERING

BY
SALAH HAFFAR

MAY 2017

Determination of Optical Constants by Using THz Time-Domain Spectroscopy

M.Sc. Thesis

in

Electrical and Electronics Engineering

University of Gaziantep

Supervisor

Prof. Dr. Uğur Cem HASAR

by

Salah HAFFAR

MAY 2017

REPUBLIC OF TURKEY

UNIVERSITY OF GAZIANTEP

GRADUATE SCHOOL OF NATURAL AND APPLIED SCIENCES

DEPARTMENT OF ELECTRICAL AND ELECTRONICS ENGINEERING

Name of the thesis: Determination of Optical Constants by Using THz Time-Domain Spectroscopy

Name of the student: Salah HAFFAR

Exam date : 26.05.2017

Approval of the Graduate School of Natural and Applied Sciences

Prof. Dr. Ahmet Necmeddin YAZICI

Director

I certify that this thesis satisfies all the requirements as a thesis for the degree of Master of Science.

Prof. Dr. Ergun ERÇELEBİ

Head of Department

This is to certify that we have read this thesis and that in our consensus opinion it is fully adequate, in scope and quality, as a thesis for the degree of Master of Science.

U.C. HASAR

Prof. Dr. Uğur Cem HASAR

Supervisor

Examining Committee Members	Signature
Assoc. Prof. Dr. Gölge ÖĞÜCÜ YETKİN	....
Assist. Prof. Dr. Furkan DİNÇER	....
Prof. Dr. Uğur Cem HASAR	U.C. HASAR

I hereby declare that all information in this document has been obtained and presented in accordance with academic rules and ethical conduct. I also declare that, as required by these rules and conduct, I have fully cited and referenced all material and results that are not original to this work.

Salah HAFFAR

ABSTRACT

DETERMINATION OF OPTICAL CONSTANTS BY USING THZ TIME-DOMAIN SPECTROSCOPY

HAFFAR, SALAH
M.Sc. in Electrical and Electronics Engineering
Supervisor: Prof. Dr. Uğur Cem HASAR
May 2017
58 pages

The Terahertz (THz) time-domain spectroscopy represents the spectrum region between the microwave and the infrared with a range between 0.1-30 THz. In recent years, the THz spectrum have received great attention of the scientific community because of its non-destructive testing properties and its unique applications in various fields. In order to effectively use the functionality of THz spectroscopy, optical properties of materials should be extracted accurately and correctly. This thesis focuses on proposing a new method for extracting optical constants of low-loss or lossless materials using reflection-only signals.

We applied the following steps for validation of our method. First, time-domain signals of the sample (Si or GaAs) with/out a perfect electric conductor (PEC) backing are simulated using a commercial 3D electromagnetic simulator program (CST Microwave Studio©). Then, appropriate windows are applied to sample out the required components of the reflected signal and transmitted signal (for comparison). Next, fast Fourier transform algorithm was implemented to transform the time-domain signal components into frequency-domain signal components. Finally, frequency-domain signal components are utilized to extract the optical properties of the analyzed sample.

The advantages of the proposed method are that it doesn't require the application of any numerical technique with an appropriate initial guess, and it uses only reflection properties so that the proposed formula is applicable to optical characterization of samples backed by a PEC.

Keywords: Optical constants, self-calibration, reflection-only, time-domain spectroscopy

ÖZET

THZ ZAMAN UZAYI SPEKTROSKOPİSİSİNİ KULLANARAK OPTİK SABİTLERİN HESAPLANMASI

HAFFAR, SALAH
Yüksek Lisans Tezi, Elektrik-Elektronik Mühendisliği Bölümü
Tez Yöneticisi: Prof. Dr. Uğur Cem HASAR
Mayıs 2017
58 sayfa

The Terahertz (THz) zaman-uzayı spektroskopi, 0.1-30 THz frekans aralığına tekabül eden mikrodalga ve infrared bölgeleri spektrumları arasında yer almaktadır. THz spektrumu, tahribatsız test imkanı sağlaması ve farklı alanlarda özgün uygulamalarda kullanılabilmesinden dolayı, yakın zamanda bilim camiasının ilgisini çekmiştir. THz spektroskopinin fonksiyonel bir biçimde kullanılabilmesi için malzemelerin optik özelliklerinin doğru ve hassas çıkarımı önem arz etmektedir. Bu tez kayıpsız ve az-kayıplı malzemelerin optik sabitlerinin çıkarımı için sadece yansıma sinyali bilgisini kullanan yeni bir yöntemin geliştirilmesi üzerinedir.

Önerilen yöntemin doğrulanması için şu adımlar uygulanmıştır. İlkin, mükemmel elektrik iletken (PEC) ile sonlandırılmış/sonlandırılmamış örneğin zaman-uzayı sinyalleri ticari 3 boyutlu bir elektromanyetik program ile (CST Mikrodalga stüdyosu©) benzeşimleri elde edilmiştir. Sonrasından, yansıyan ve iletilen sinyallerin (karşılaştırma için) istenilen bileşenleri uygun pencere ile örneklenmiştir. Ardından, zaman-uzayı sinyal bileşenleri frekans-uzayı bileşenlerine hızlı Fourier transfromu algoritması kullanılarak çevrilmiştir. Son olarak, frekans-uzayı sinyalleri kullanılarak analiz edilen örneğin optik özellikleri çıkarılmıştır.

Önerilen yöntemin avantajları, uygun başlangıç şartına sahip her hangi bir nümerik yöntemin uygulanmasına ihtiyaç duymaması ve yöntemin uygulanmasında sadece yansıma ölçümleri kullanıldığı için PEC ile sonlandırılmış örneklerin optik karakterizasyonu için uygulanabilir olmasıdır.

Anahtar kelimeler: Optik sabitler, öz-kalibrasyon, sadece-yansıma, zaman-uzayı spektroskopisi

To My Family…

ACKNOWLEDGEMENTS

I would like to thank my supervisor Prof. Dr. Uğur Cem HASAR for his helpful guidance and support through the completion of this thesis. He introduced me to this subject and explained the ambiguity that I faced untill the end of this work.

I would like also to thank the Scientific and Technological Council of Turkey (TUBITAK) for providing a budget for the commercial 3D Electromagnetic simulation program – the CST Microwave Studio.

Finally, I would like to thank my family for their endless support and encouragement until the final steps of finishing this work.

TABLE OF CONTENTS

LIST OF TABLES

Page

LIST OF FIGURES

Page

CHAPTER 1

INTRODUCTION

Over the last decades the THz technologies has received a lot of interests among scientists due to its applications and benefits in various fields. THz spectroscopy has been applied in different areas, including bio-medical, pharmaceutical, security, and non-destructive testing . The research interests have focused on the generation and detection the THz spectroscopy for the aforementioned. In our work we will be focusing on proposing a method that can be used in non-destructive applications.

1.1 Definition of THz spectroscopy

The THz region is the electromagnetic spectrum whose frequency lies in between the microwave and infrared region of the spectrum with a commonly used frequencies across (0.1-30) THz [1].

1.2 Terahertz Band

The Terahertz band is the spectrum of the THz region radiation. Some researcher communities called it Terahertz radiation and thats simillalry to micowave, x-ray, and Infrared radiations [1]. Others called it the T-ray which is the most common name among researchers[1]. The Figure 1.1 [1] shows the T-ray band spectrum with its mostly used parameters.

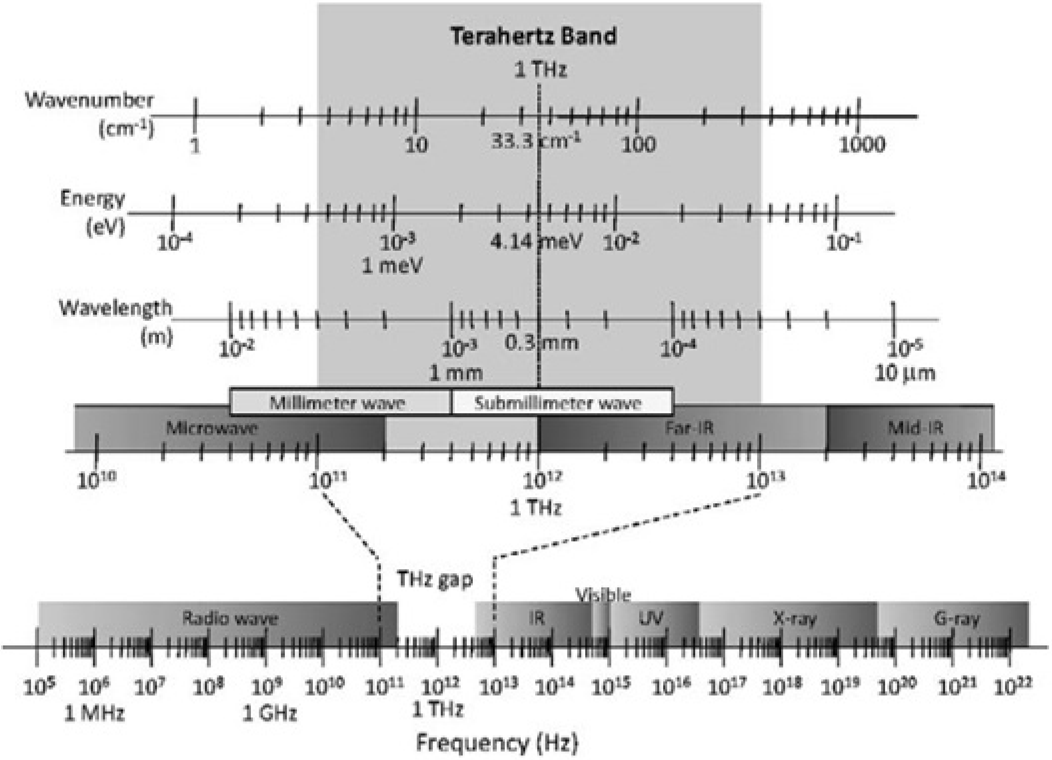

Figure 1.1: The T-ray Band electromegnatic spectrum

From Figure 1.1 we can define some basic definitions as the following:

- Frequency: f = 1 THz = 1000 GHz .
- Angular frequency ω = 2 $\pi f \approx$ 6.28 THz .
- Period : τ= 1/f = 1 ps.
- Wavelength : = $c/f \approx$ 0.3 mm.
- Photon energy : hf = $h\omega = 4.14 meV.$
- Wave Number : $\overline{k}$ = $k/2\pi$ = 33.3 $cm^{-}1$.
- Temperature : T = $hf/$ $k_s = 48K.$

where c denotes the speed of light in space, h is the Planks' constant, and k_s is the Boltzmanns constant.

1.3 THz Applications

There are a verity of application that uses the T-ray spectroscopy and we can explain this usage breifly as follows:

1.3.1 Pharmacitical Industry

The THz spectroscopy can be used to perform coating to drug tables by taking a 3D image and apply an analysis to it to examine the thickness and integrity and to identify the perfect localization of the chemical and phisical structure of the sample under scanning [2].

1.3.2 Medicine and Biology

Lots of studies showed the benefits of using the T-ray spectroscopy in the medical and biological feilds. For exsample using the terahertz radiations to inter molecular and intramolecular vibrations to enable the investigations of the crystalline state of a drug [2]. Similar to X-rays , terahertz radiations have a low photonic energy which doesn't cause a harmful damage to the human's tissues so some of the terahertz frequencies with its capability of penetrating can be used for detecting the differences in the water content and tissue density [2]. The THz spectroscopy can also be used for detecting the molecular interactions that occur in the compunds formed by the hydrogen bonds and hydration reactions, Figure 1.2 shows the detection of the molecular bonds [3].

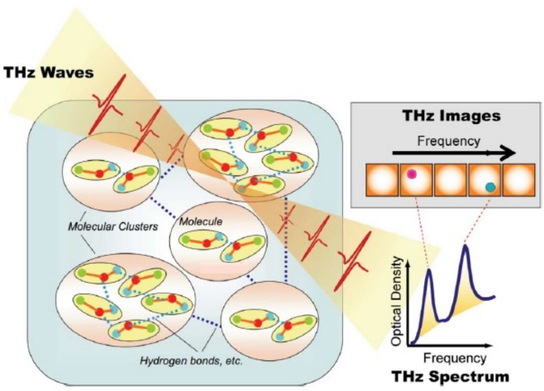

Figure 1.2: A THz spectroscopy relation with different molecular bonds

1.3.3 Cultural Heritage

Because THz spectroscopy has a non-destructive propority, a lot of researchers used a wide range of THz frequency spectrum that can penetrate plaster, wood and ceramics [4] . Than to this properties it can show valuable information about the life history and construction of the studied samples.

1.3.4 Security and Quality Inspection

Harmful objects that have been hidden in several kind of clothes or fabrics can be detected by using different THz band frequencies [5]. On the other hand concealed objects can be investigated by measuring the radiometric temperature under the human clothing using the terahertz imaging by using broadband different terahertz images [7]. Figures 1.3 [5] and 1.4 [2] illustrate the scanning application of the technique.

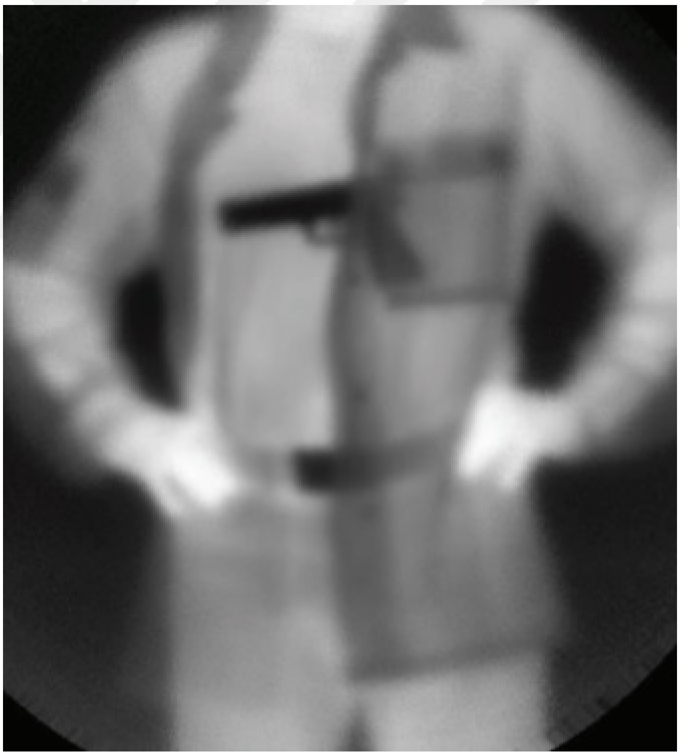

Figure 1.3: A (0.85-THz) image by THz camera depict the ability of showing the objects through clothes or fabric

Figure 1.4: A THz spectroscopy detector showing a man holding a hidden knife

The THz spectroscopy can by applied to detect strange unwanted metal, glass, sharp object through a production line which can't be otherwise detected by using the traditional x-ray detectors. As a result the THz radiation can be used as a quality inspector during the production [6]. The Figure 1.5 [6] shows an example of a detected object over the production line.

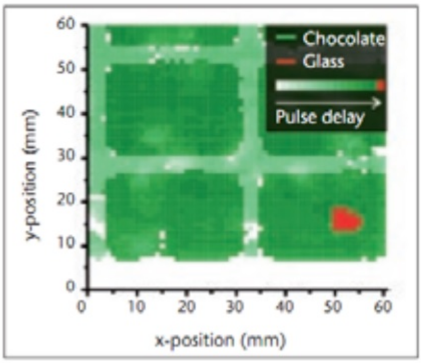

Figure 1.5: A detected piece of glass within a bar of chocolate using THz spectroscopy

1.3.5 Gas Sensing

The THz spectroscopy is used for gas sensing to monitor gas emission of different vehicles and factoris gas emission. Via gas absorption by a terahertz spectrometer [8].

Besides measuring the gas temperature using different frequency range of the THz spectroscopy can be another application [9].

1.3.6 Telecommunications

Due to the increasing needs for bigger bandwidth and higher data rates which will exceed the 10 Gbit/s [10], it is considered the THz spectroscopy will be the future candidate spectrum to deal with this huge amount of data needed to transfer with a frequency range of 110 - 170 GHz (D-band) or range of 300 - 350 GHz. With a wider terahertz range, it is possible to attain higher speeds to the wireless links which will give a various and wide number of applications such as wireless short-range communications, body communication systems for health monitoring, and providing secure defense wireless communication equipment for military purposes [11].

1.3.7 Materials Characterization

The THz spectroscopy can be used to characterize different materials by measuring the difference between refractive indexes of various materials [12]. On the other hand the THz spectroscopy can be used to measure the density of the lubricating oils due to their low absorbance characteristic in the infrared region [12].

1.4 Thesis Outline

After introducing the definition and some main applications of the THz spectroscopy, the rest of our work is organized as follows:

- **Chapter 2**: In this chapter, we will discuss previous contributions related to our work and investigate the main advantages and limitations of each study.
- **Chapter 3**: We will then introduce our methodology by using the appropriate equations and derivations to implement our self-calibration technique.
- **Chapter 4**: After finishing the theoretical studies we will validate our work using different samples and calculations from a simulation software data and compare it with the real result with an appropriate discussions.

- **Chapter 5**: We will make a conclusion of our work and discuss a potential future work related to our study.

CHAPTER 2

LITERATURE REVIEW OF PREVIOUS STUDIES IN THZ TIME-DOMAIN SPECTROSCOPY

The past two decades have witnessed a lot of interest in studying the THz time-domain spectroscopy because of its various superior properties mentioned in the previous chapter. There are two major concerns that the researchers are interested in this field; 1) The derivation and calculation of the studied material Optical constants' and 2) calculations of the material sample thickness. In this chapter we will review the previous contributions based on these two categories.

2.1 Calculations of The Optical Constants

Many studies were presented to either extract the optical constants or to apply the THz radiation for measuring the refractive index of the testing sample. The THz time-domain spectroscopy is characterized by two major modes : the transmission mode and reflection mode. Figure 2.1 shows the reflection mode of the THz spectroscopy.

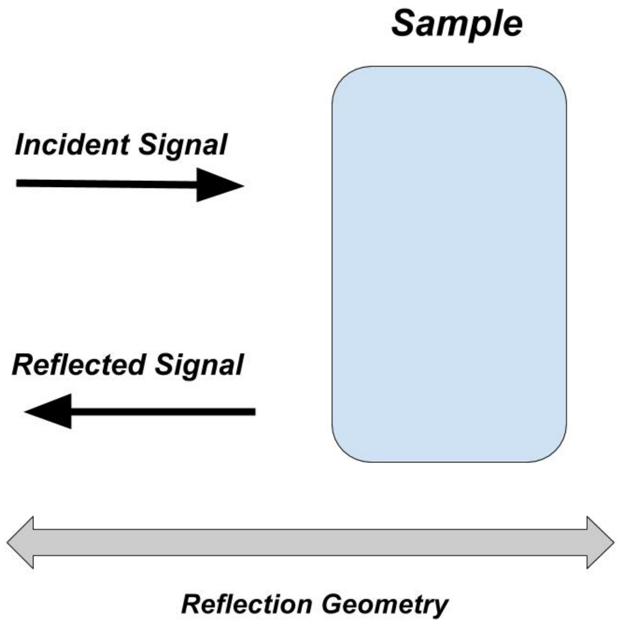

Figure 2.1: Transmission and reflection regions

Moller *et al.* [13] used the reflection geometry characteristics to calculate the index of refraction in a solution by dividing a reflected signal between a receiver and a testing liquid by a reference reflected signal between air and a receiver. Another study using the reflection geometry was done by Zhong *et al.* [14] to classify different types of chemical substances by dividing a reflection signal on an incident beam signal. These two techniques require the information of reference signals.

Like the reflection geometry, many other techniques were presented in the past few years following the transmission mode which is shown in Figure 2.2 . Some algorithms in the transmission mode were relying on the testing sample thickness and others were using a reference signals to obtain the transfer function.

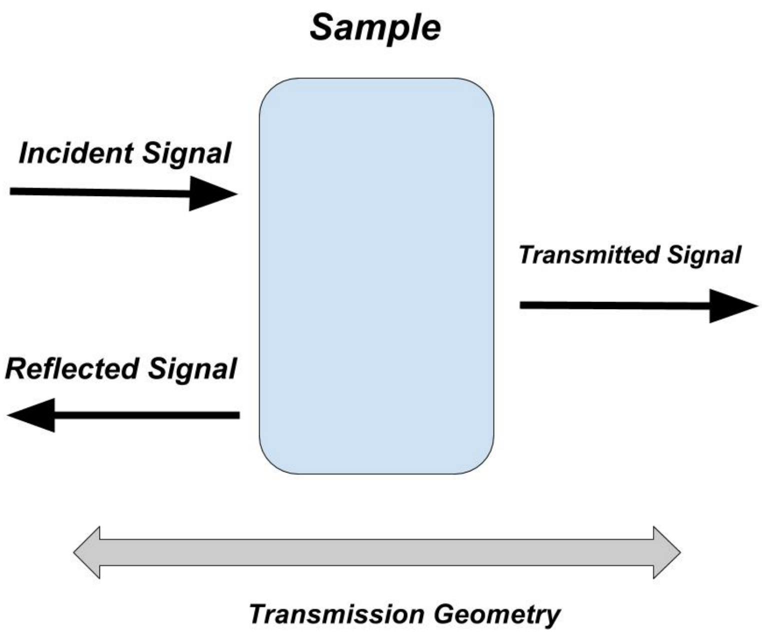

Figure 2.2: Transmission mode geometry

Duvillaret *et al.* [15] [16] proposed a numerical method to extract the optical constants based on a pre-known sample thickness. However, the accuracy of this technique depends on the closeness of the estimated sample thickness to the actual sample thickness. Another technique to obtain the material's optical parameters was presented by Dorney *et al.* [17] in which they calculate the material parameters by using a reference signal data to form their transfer function, but the main issue with this method is the accuracy depending on the precise measurement of the reference signal. On the other hand, Pupeza *et al.* [18] proposed another work related to the method proposed by [16] in order to increase accuracy by measurements applied with special filter. The useage of this added fiters' measurements however will lead to much more complexity and will increace the time consumed to obtain the results. In order to overcome the need for reference measurement , Hejase *et al.* [19] presented a self-calibrated technique to obtain the optical constants, but again the accuracy of the method will decrease by the inaccurate sample thickness choice. Lately, Singh *et al.* [20] presented an algorithm to calculate the optical parameters using the information of four transmission and reflection data signals without the need for sample thickness or reference signal data.

2.2 Sample Thickness Estimation

Besides extraction of optical constants extraction, researchers have an interest to estimate the sample thickness simultaneously with the calculation of optical constants. Figure 2.3 shows a typical geometry for evaluation of sample thickness. One way to extract estimate the sample thickness [16] is to measure the echoes obtained from the measured data along with measurement of the optical constants. However, this calculation procedure is susceptible to incorrect measurements due to the need of the pre-known sample thickness. Another way proposed to estimate the sample thickness [17] and [21] relies on extraction of the sample thickness iteratively by multiple calculations within the studied frequency. The main drawback of these methods is that the iterative calculations are time consuming when applying calculations mutiple times. In order to eliminate the need for pre-determined thickness and reference measurement data, [20] used a method to calculate the sample thickness by using the received reflected data from the sample.

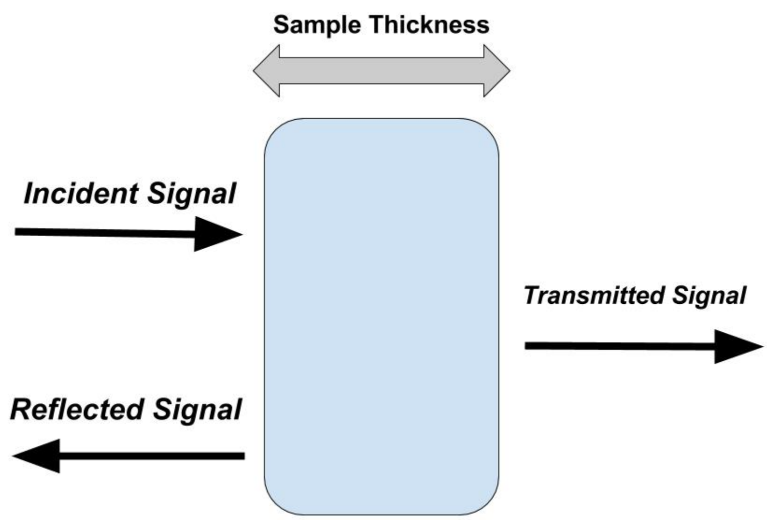

Figure 2.3: General Sample Thickness

2.3 Motivation of our work

In our work we will be demonstrating a THz non-iterative time domain spectroscopy technique using only the measurements of three reflected signals with no need to sample thickness knowledge, reference signal, or transmission data information.

CHAPTER 3

EXTRACTION OF THE OPTICAL CONSTANTS AND SAMPLE THICKNESS USING THZ SPECTROSCOPY

In this chapter we will firstly review fundamentals of the electromagnetic equations. Then, we will show basic relations of the reflection and transmission of a surface. Finally, we will extract the optical constants based on our proposed method.

3.1 Basic Electromagnetic Field Equations

The Electromagnetic field in general is described by the following Maxwell equations [22] :

$$\nabla.\vec{D} = \rho, \tag{3.1}$$

$$\nabla.\vec{B} = 0, \tag{3.2}$$

$$\nabla \times \vec{E} = -\frac{\partial \vec{B}}{\partial t}, \tag{3.3}$$

$$\nabla \times \vec{H} = \vec{J}_f + \frac{\partial \vec{D}}{\partial t}, \tag{3.4}$$

the equations above represent relations between the electric and magnetic fields and sources (charge and current densities). Here, ∇ denotes the three-dimensional gradient operator (see Appendix A), the $\vec{E}$ and $\vec{B}$ are the electric and magnetic fields, and ρ denotes the (free) charge density. $\vec{J}$ is the (free) current density in a specific medium, $\vec{D}$ and $\vec{B}$ are the displacement electric and magnetic fields expressed by :

$$\vec{D} = \epsilon_0\vec{E} + \vec{P} = \epsilon\vec{E}, \tag{3.5}$$

$$\vec{B} = \mu_0 \vec{H} + \vec{M} = \mu \vec{H}, \tag{3.6}$$

$$\vec{J} = \sigma \vec{E}, \tag{3.7}$$

where ϵ_0 and μ_0 are the electric permittivity and magnetic permeability in free space. ϵ=ϵ_0 ϵ_r and μ= μ_0 μ_r where ϵ_r and μ_r are the material relative permittivity and permeability, $\vec{P}$ and $\vec{M}$ are the polarization and magnetization vectors of the medium, and σ describes the conductivity of the medium. Assuming that the medium is linear, isotropic, homogeneous, and its constitutive properties are non-time varying [22], and by applying the curl terms to both sides of the equation (3.3) we obtain

$$\nabla \times \nabla \times \vec{E} = -\mu_0 \frac{\partial}{\partial t}(\nabla \times \vec{H}), \tag{3.8}$$

$$\nabla^2 \times \vec{E} = -\nabla \times \nabla + \nabla(\vec{\nabla}.\vec{E}) \tag{3.9}$$

In free space ρ =0 , σ= 0 and the equation (3.9) simplifies to

$$\nabla^2 \vec{E} = -\mu_0 \epsilon_0 \frac{\partial^2 \vec{E}}{\partial t^2}. \tag{3.10}$$

The equation (3.10) represents the wave equation of the electric field in free space showing spatial and temporal dependence. A typical picture of the electric and magnetic fields is shown in Figure 3.1.

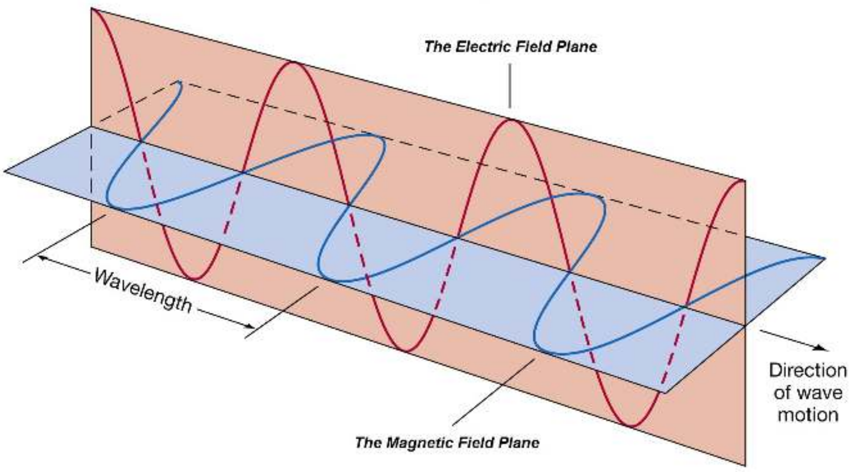

Figure 3.1: The electrical and magnetic wave planes

3.2 Transmitted and Reflected Waves

In the previous section we assumed that the wave is traviling in an unbounded free space, but in general the electromagnetic wave travels through various interfaces and mediums. When the electromagnetic wave propagates, it will encounter scattering and attenuations [23]. For these reasons, a study on transmission and reflection at an interface becomes important. The electromagnetic wave is composed of phase and amplitude. Therefore, the transmitted and reflected waves are expressed as complex quantities. In our study we will be considering the plane wave propagation in which the electric plane is perpendicular on the magnetic plane, and we will assume that the incident angle equal to zero(normal incidence).

3.2.1 Lossless Medium Incidence

We assume that an incident wave is incident to a planar boundary interface. Both media (before and after the planar) have interface their own characterized constitutive relations related to both permittivity and permeability. So the permittivity and permeability for the first medium are ϵ_1 and μ_1, and for the second medium ϵ_2 and μ_2 , respectively. When the incident wave impinges to the surface, part of the wave will reflect back from the surface and its remaining part be transmitted through the surface. Figures 3.2 shows the incident, reflected, and transmitted wave signals. The electric field in this configuration is polarized in the *x* direction and the propagation is in the z direction. In our analysis we consider $e^{j\omega t}$ time dependence. Then, we find the following [24]

$$\vec{E_i} = \hat{a_x} E_0 e^{-j\beta_1 z}, \tag{3.11}$$

where β=$\omega^2\epsilon\mu$ is the phase constant and E_0 is the amplitude of the incident electric field.

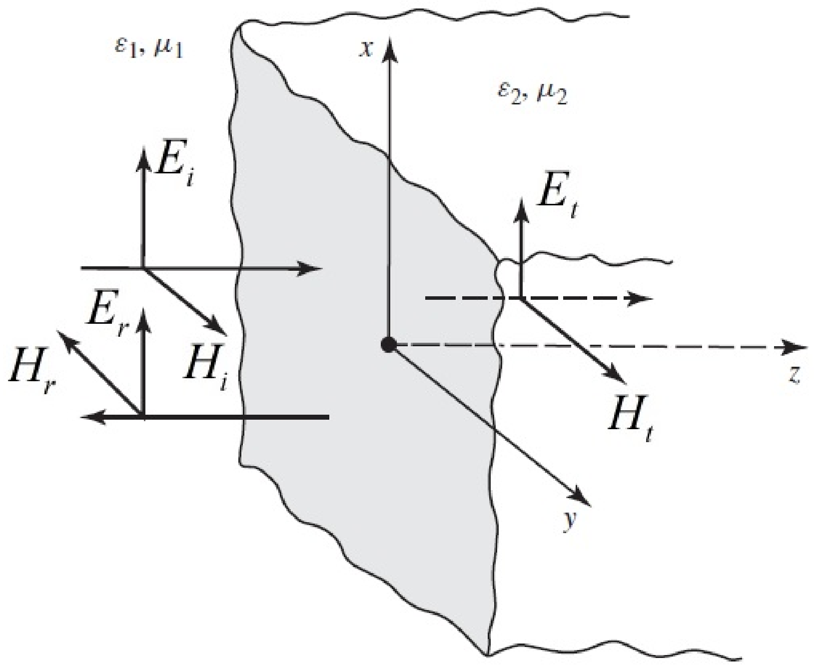

Figure 3.2: Transmitted and reflected Waves

Because the interface is flat, polarization of reflected and transmitted waves will not change [22].Then, the reflected and transmitted waves can be expressed as the following:

$$\vec{E_r} = \hat{a_x} r E_0 e^{j\beta_1 z}, \tag{3.12}$$

$$\vec{E_t} = \hat{a_x} t E_0 e^{-j\beta_2 z}, \tag{3.13}$$

where *r* and *t* are the reflection and transmission coefficients at the interface, respectively . The values of the reflection and transmission coefficients are unknown and can be determined by applying the boundary conditions between medium 1 and medium 2. Because of the plane wave propagation and the assumption of the planar wave incidence, we will assume that the polarization of the reflected and transmitted waves are having the same polarization as the incident wave which have a linear polarization. Considering the same procedure as we did with the electric field we obtain the incident, reflected, and transmitted waves on the *y* plane for the magnetic field as the following

$$\vec{H_i} = \hat{a_y} \frac{H_0}{\eta_1} e^{-j\beta_1 z}, \tag{3.14}$$

$$\vec{H}_r = -\hat{a_y}\frac{rH_0}{\eta_1}e^{j\beta_1 z}, \tag{3.15}$$

$$\vec{H}_t = \hat{a_y}\frac{tH_0}{\eta_2}e^{-j\beta_2 z}, \tag{3.16}$$

where $\eta_1 = \sqrt{\mu_1/\epsilon_1}$ and $\eta_2 = \sqrt{\mu_2/\epsilon_2}$ are the intrinsic impedance of the medium 1 and medium 2, respectively. To obtain both reflection and transmission coefficients we apply the boundary condition by equating the tangential components of electric and magnetic fields at the tangent at interface (z=0) then, we find

$$E_0 e^{j\beta_1(0)} + rE_0 e^{-j\beta_1(0)} = tE_0 e^{j\beta_2(0)}, \tag{3.17}$$

$$E_0(1+r) = tE_0, \tag{3.18}$$

So

$$1 + r = t. \tag{3.19}$$

Similarly applying the boundary conditions to the $\vec{H}$ field we find

$$\frac{1}{\eta_1}(1-r) = \frac{1}{\eta_2}t \tag{3.20}$$

By solving the equations (3.19) and (3.20) for both reflection and transmission coefficients we obtain

$$r = \frac{\eta_2 - \eta_1}{\eta_2 + \eta_1}, \tag{3.21}$$

and

$$t = \frac{2\eta_2}{\eta_1 + \eta_2}, \tag{3.22}$$

The generalized equations above called the Frensel equations for reflection and transmission for a plane wave with no incident angle. In our study we considered non-magnetic medium. The complex refractive index is given by $n = \sqrt{\epsilon\mu}$ and for the non-magnetic medium the complex refractive index equals to $n = \sqrt{\epsilon}$. The intrinsic impedance for a non-magnetic medium is $\eta = 1/\sqrt{\epsilon}$ and that yields to $\eta = 1/n$. By substituting $\eta = 1/n$ in the equations (3.21) and (3.22) we obtain

$$r_{ij} = \frac{n_i - n_j}{n_i + n_j}, \tag{3.23}$$

and

$$t_{ij} = \frac{2n_i}{n_i + n_j}. \tag{3.24}$$

The equations (3.23) and (3.24) represents the transmission and reflection coefficients in term of the complex refractive index.

3.3 Wave Propagation Through A Sample

In the previous subsection, we studied the reflection and the transmission properties of a certain interface. In this section we will first investigate the effect of wave propagation through a sample. Then we will analyse reflection characteristics of a sample backed by a perfect conductor (shorted sample).

3.3.1 Reflection and Transmission of a Sample Properties

Figure 3.3 illustates a sample immeresed in air regions (ϵ_0 ,μ_0, σ_0) for analyzing its reflection and transmission properites (free-space analysis). THz source of signal is placed at the end *A*, the distance between *A* and the left surface of the sample is denoted as d_1, the thickness of the sample is d, and the distance between the right surface of the sample and the *B* end will be denoted as d_2. When the incident wave from the THz source passes through the sample, it will be subject to a discontinuity. So when the signal collides with the left interface of the sample, part of the signal will be reflected at the interface and its remaining part will be transmitted into the sample to produce a transmitted signal at the end of the same model. The THz signal transmitted into the sample will receive mutiple reflections within the sample, which is called by the Fabry-Perot phenomena [18] [24]. Both the *A* and *B* ends will receive infinity many numbers of reflected and transmitted wave signals. But, generally only five to six amplitudes can be detected sufficiently due to loss nature of the sample.

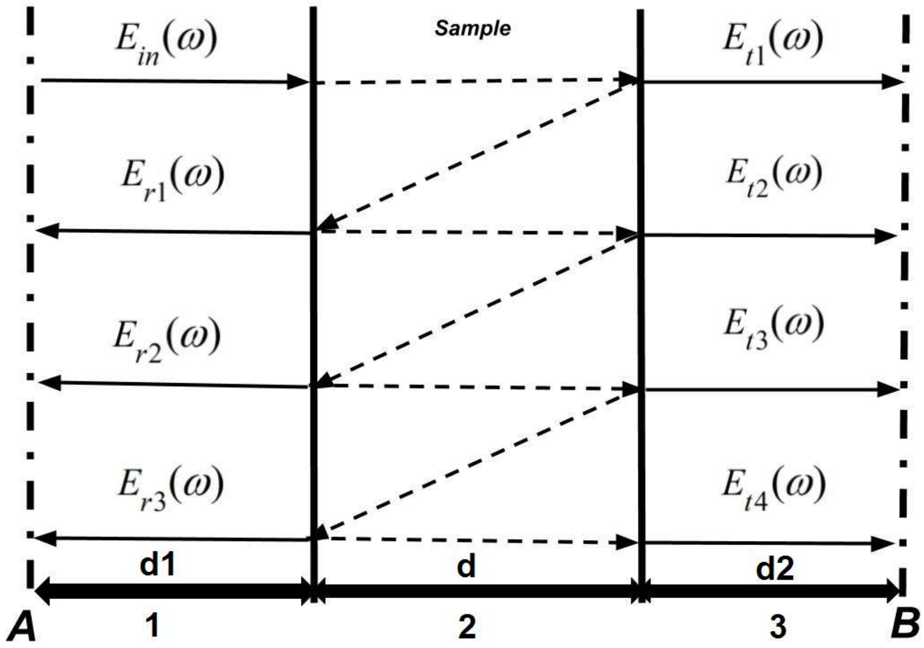

Figure 3.3: Transmission and reflection waves in a homogenous medium

Since we are interested in reflection and transmission properties of the sample in Figure 3.3. And because only few reflected and transmitted signals are needed in our theoretical model, we can apply the ray-tracing technique [25]. According to this technique the frequency domain for two transmitted signals can be expressed as

$$E_{t1}(\omega) = E_{in}(\omega)t_{12}t_{23}TR_1R_2, \tag{3.25}$$

$$E_{t2}(\omega) = E_{in}(\omega)t_{12}r_{23}r_{21}t_{23}T^3R_1R_2. \tag{3.26}$$

In a similar fashion, the first three frequency-domain reflected signals can be given as

$$E_{r1}(\omega) = E_{in}(\omega)r_{12}R_1^2, \tag{3.27}$$

$$E_{r2}(\omega) = E_{in}(\omega)t_{12}r_{23}t_{21}T^2R_1^2, \tag{3.28}$$

$$E_{r3}(\omega) = E_{in}(\omega)t_{12}r_{21}r_{23}^2t_{21,}T^4R_1^2. \tag{3.29}$$

Where

$$T = e^{-j\theta} \qquad \theta = \omega n_{sam} d/c$$

$$R_1 = e^{-j\theta_1} \qquad \theta_1 = \omega n_{air} d_1/c$$

$$R_2 = e^{-j\theta_1} \qquad \theta_1 = \omega n_{air} d_2/c$$

In the equations above the $E_{in}(\omega)$ is the incident waves , r_{12} represents the reflection coefficiant between regions 1 and 2 , r_{21} represent the reflection coefficiant between regions 2 to 1, and r_{23} represent the reflection coefficiant between regions 2 to 3. In the same manner, the t_{12}, t_{21}, and t_{23} represents the transmission coefficiants between regions 1 to 2 , 2 to 1 , and 2 to 3 , respectively. n_{sam}, n_{air} are the complex refractive index of the sample and air, respectively. The complex refractive index is given as $n = n_{real} + jn_{imag}$, where n_{real} is the real part of the refractive index and n_{imag} is absorption index which equals to k= α λ_0 /4π , where α is the absorption constant and λ_0 is the wavelength is free space [27]. c is the speed of light in a vacuum , ω is the angular frequency. n_{air} and n_{sam} denote the complex refractive index of air and the sample. In the study [20] two reflected frequency-domain and two transmitted frequency-domain signals were used to extract the refractive index of the sample using calbration-independent data (no need for the values R_1 and R_2). In this thesis, we will accomplish the same goal (determination of the refractive index of the sample using calbration-independent data), by utilizing three frequency-domain reflected signals only [24]. From equations (3.27) to (3.29) we obtain

$$\frac{E_{r2}^2(\omega)}{E_{r1}(\omega)E_{r3}(\omega)} = \frac{E_{in}^2(\omega)t_{12}^2 r_{23}^2 t_{21}^2 T^4 R_1^4}{r_{12}t_{12}r_{21}r_{23}^2 t_{21} E_{in}(\omega)^2 T^4 R_1^4} \tag{3.30}$$

After cancelling the common parameters we find

$$\frac{E_{r2}^2(\omega)}{E_{r1}(\omega)E_{r3}(\omega)} = \frac{t_{12}t_{21}}{r_{12}r_{21}} \tag{3.31}$$

The previous equation is the simplest formula that consists of two only two reflection and two transmission coefficients. Assuming that the sample is a dielectric sample, then equations (3.23) and (3.24) for a lossless sample reduce to

$$\frac{t_{12}t_{21}}{r_{12}r_{21}} = \frac{\frac{2n_1}{n_1+n_2} \cdot \frac{2n_2}{n_1+n_2}}{\frac{n_1-n_2}{n_1+n_2} \cdot \frac{n_2-n_1}{n_2+n_1}} = \frac{4n_1n_2}{(n_1-n_2)(n_2-n_1)},$$

Since $n_{sam} = \sqrt{\epsilon\mu}$ and $n_{air} = \sqrt{\epsilon_0\mu_0}$ so

$$\frac{E_{r2}^2(\omega)}{E_{r1}(\omega)E_{r3}(\omega)} = \frac{4n_{air}n_{sam}}{(n_{sam}-n_{air})(n_{air}-n_{sam})} = M \tag{3.32}$$

Here M is a linear parameter obtained from suitable gating of the reflected signal, to be mentioned in Chapter 4. For simplicity we assume that the complex refractive index of air equals to n_{air} =1- 0*j* so

$$n_{sam}^2 M - n_{sam}(2M-4) + M = 0. \tag{3.33}$$

By solving equation (3.33) we obtain

$$n_{sam} = n_{real} - jn_{imag} = \frac{(M-2) \mp \sqrt{(M-2)^2 - M^2}}{M} \tag{3.34}$$

Because we are dealing with the determiation of complex refractive index of conventional materials, we consider $n_{real} \geq 1$ for the $e^{j\omega t}$ time reference. However, it should be point that for metamaterials (engineered materials constructed by special arangment conventional materials) n_{real} can be less than zero [26], which is not considered in this thesis. Besides the imaginary part of the refractive index must be grater than or at least equal to zero $n_{imag} \geq 0$ for the $e^{j\omega t}$ time reference [26]. By using this algorithm it can be easy to calculate the optical constants of a homogeneous medium. When we compare the expression of n_{sam} in equation (3.31) in this thesis with the equation (10) in [20] we notice that they are identical. However, the advantage of out technique is that it allows the same calculation of n_{sam} by using only three reflected signals, instead of four reflected and transmitted signals as in [20]. Another advantage of our technique is that it doesn't necessitate the usage of any reference signal as used in [17] .

3.3.2 Reflection Properties of a Shorted Sample

As derived above, our proposed technique uses only the reflected wave signals with no need for transmission signal informations. In this regard, our technique is specially useful for the determination of complex refractive index of samples backed by a perfect electric conductor (PEC). Figure 3.4 illustrate a configuration of a sample terminated in a PEC for analysing its reflection properties. Here, part of the wave propagated from the THz source which has been placed at the *A* end impinges on the sample there by causing reflection to the *A* end, and the other part will be transmitted into the sample causing the aforementioned Fabry-Perot effect. When the travelling wave reaches the right end of the sample, it will not continue its transmission to the *B* end due to the existence of the PEC plate but instead it will just produce multiple reflection in the sample.

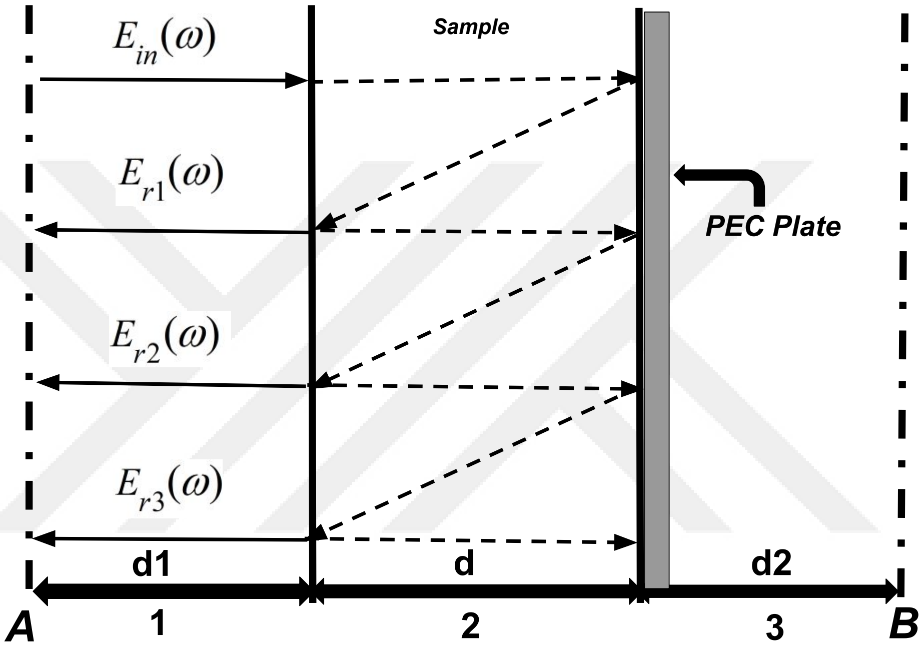

Figure 3.4: Reflected waves in a homogenous medium with PEC plate

No transmitted signals from medium 2 to medium 3 means $t_{23} = 0$. By substituting it in equations (3.25) and (3.26) we find

$$E_{t1}(\omega) = E_{in}(\omega)t_{12}(0)TR_1R_2 = 0, \tag{3.35}$$

$$E_{t2}(\omega) = E_{in}(\omega)t_{12}r_{23}r_{21}(0)T^3R_1R_2 = 0. \tag{3.36}$$

So we can see that $E_{t1}(\omega) = E_{t2}(\omega) = 0$. It means that $r_{23} = -1$ since $r_{23} = t_{23} - 1$. Substituting $t_{23} = 0$ into equations (3.27) to (3.29) we find that

$$E_{r1}(\omega) = E_{in}(\omega)r_{12}R_1^2, \tag{3.37}$$

$$E_{r2}(\omega) = E_{in}(\omega)t_{12}(-1)t_{21}T^2R_1^2, \tag{3.38}$$

$$E_{r3}(\omega) = E_{in}(\omega)t_{12}r_{21}(-1)^2t_{21,}T^4R_1^2. \tag{3.39}$$

Thus for $r_{23} = -1$ we have

$$\frac{E_{r2}^2(\omega)}{E_{r1}(\omega)E_{r3}(\omega)} = \frac{E_{in}^2(\omega)t_{12}^2(-1)^2t_{21}^2T^4R_1^4}{r_{12}t_{12}r_{21}(-1)^2t_{21}E_{in}(\omega)^2T^4R_1^4}, \tag{3.40}$$

resulting in

$$\frac{E_{r2}^2(\omega)}{E_{r1}(\omega)E_{r3}(\omega)} = \frac{t_{12}t_{21}}{r_{12}r_{21}}. \tag{3.41}$$

We see that the result in equation (3.41) has the same formula as in equation (3.31). What it means is that we can follow the same procedure discussed in subsection 3.3.1 to determine the complex refractive index of the sample n_{sam}. Specifically we can use equation (3.34) and apply the passivity principle to ascertain the convert complex refractive index of the conventional samples.

Summing all advantages of our proposed method are that it doesn't require the application of of any numerical technique with an appropriate initial guess, and it uses only reflection properties so that the proposed formula is applicable to materials characterization of samples backed by a PEC. However, the accuracy of our proposed method will decrease with the increment of the loss of the sample since it utilizes three frequency domain reflected signals. In addition, our method needs that there must be sufficient time delay between every measured reflected signals components in order to separate the multiple signals to be discussed in subsection 4.1.1.

CHAPTER 4

SIMULATION AND VALIDATION RESULTS

In this chapter we will validate our proposed technique by using some simulation. Toward this end as shown in Figure 4.1, we will first obtain by using a commercial 3D Electromagnetic simulation program the time domain responses of two configurations: a) the sample without any backing end and b) the sample backed by a perfect electric conductor (PEC). Then, we will apply rectangular time gating to sample the required reflected and transmitted components. Next, we will apply the fast Fourier transform (FFT) to convert the time-domain gated reflected and transmitted components into frequency-domain components. Finally, we will apply equation (3.33) to determine the frequency-dependent optical constants of the two samples with different electromagnetic properties.

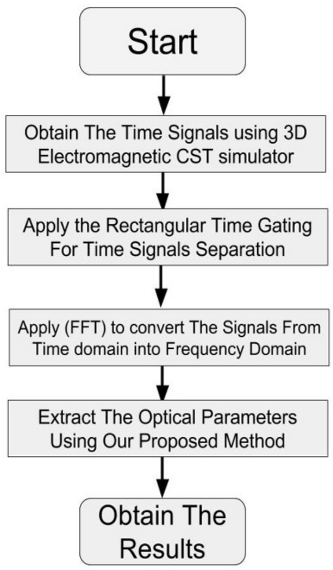

Figure 4.1: Results obtaining flow chart

4.1 Simulation Setup

To obtain our simulations, we used a three-dimensional full wave simulator Computer Simulation Technology Microwave Studio (CST-MWS) [28]. The CST software uses the mesh cell to calculate the transient wave propagation through a specific medium. We used the time-domain built-in solver to obtain our results for gathering time-domain reflected and transmitted signals components.

4.1.1 Simulation of Time-Domain Signals

To obtain the same geometry we studied in subsection (3.3.1) we build the computational volume shown in Figures 4.2 and 4.3. Both ports 1 and 2 will receive the reflection and transmission time signals. specifically, an incident signal transmitted from port 1 will collide and pass through the sample to reach port 2 to produce transmitted signals, while reflections into port 1 will constitute reflected signals. And because of that multiple signals will appear on both ports.

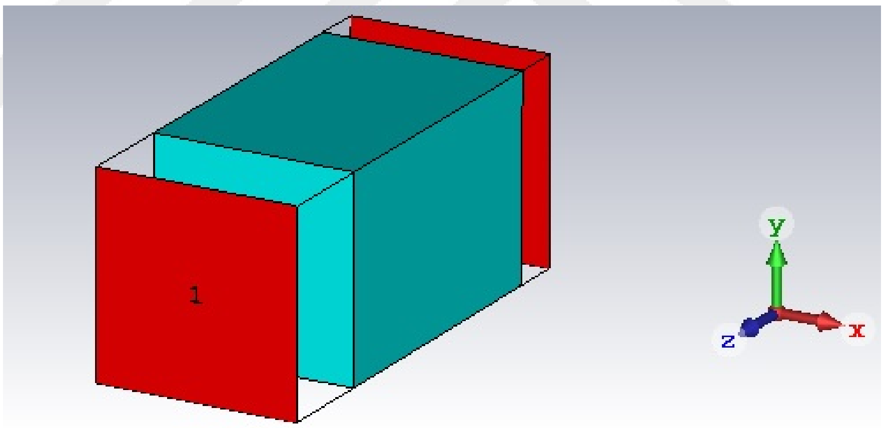

Figure 4.2: Si Sample with d_1= 1 mm and d_2= 0.5 mm

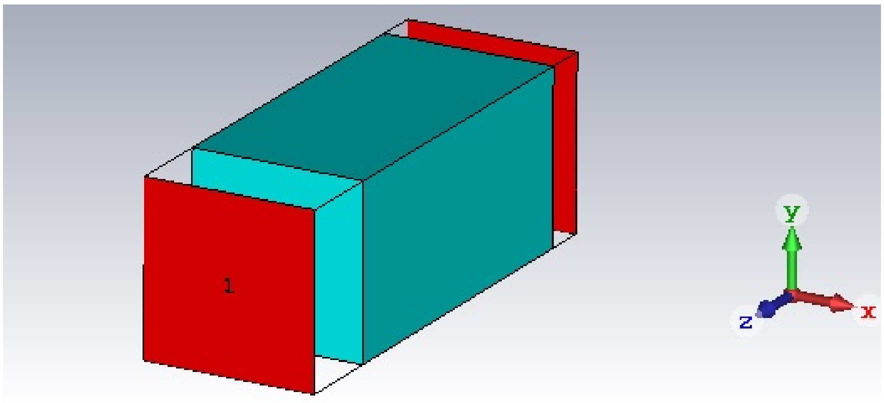

Figure 4.3: GaAs Sample with d_1= 1 mm and d_2= 0.5 mm

With the same procedure we built the computational volume as shown in Figures 4.4 and 4.5 to analyze reflection properties of a sample backed by a PEC plate. As mentioned before that the incident wave propagated through the sample from port 1 will not propagate into the next port 2 because of the PEC shorts out electric signals. Instead, such a configuration results in reflected signals in reflected signals reaching port 1.

For shorting the sample in CST we used a perfect electric conductor (PEC) plate and placing it between the sample and port 2 to ban any transmission from the sample toward the port 2.

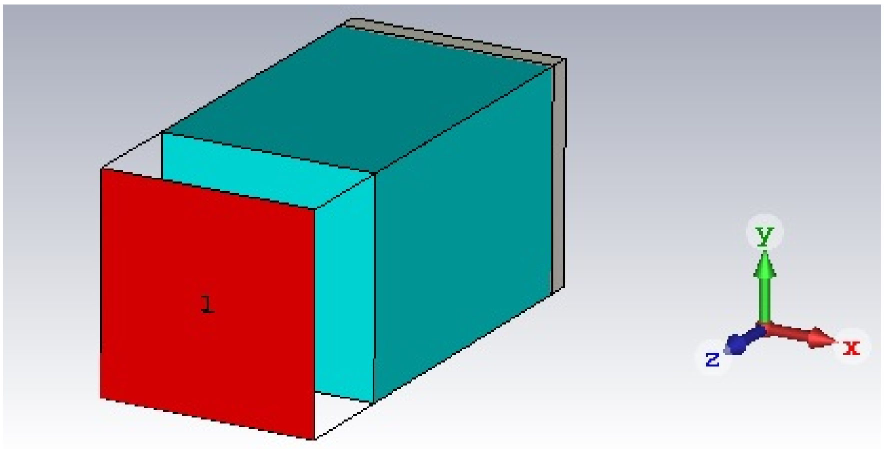

Figure 4.4: Si shorted sample with d_1= 1 mm

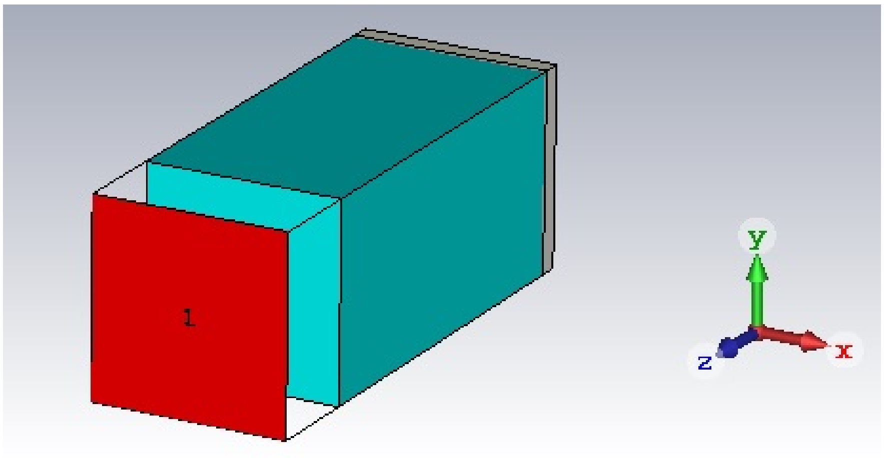

Figure 4.5: GaAs shorted sample with d_1= 1 mm

In order to insure the plane wave propagation, appropriate boundary conditions must be applied. A plane wave with polarization in the *x* direction and wave propagation in the *z* direction was assumed in our simulation. For both geometries in Figure 4.2 and 4.3. Similarly, for both geometries in Figures 4.4 and 4.5. We considered the perfect electric conductors for the propagation in the *x* direction, and perfect magnetic conductor in the *y*, and wave guide ports 1 and 2 in the *z* direction (reflection and transmission properties). To test our method we used two different types of materials with two different sample thickness. The first is Silicon(Si) which has a refractive index of n_{Si}= 3.42-*j*0 and the second one is Gallium arsenide (GaAs) which has a refractive index of n_{GaAs}= 3.61-*j*0 , Tables 4.1 and 4.2 show our samples' geometry parameters.

Sample	Refractive Index (n)	Thickness (mm)	Dimensions (mm $\times$ mm)
Si	3.42-*j*0	3	2×2
GaAs	3.61-*j*0	4	2×2

Table 4.1: Samples parameters

Sample	Refractive Index (n)	Thickness (mm)	Dimensions (mm $\times$ mm)	PEC Thickness (mm)
Si	3.42-*j*0	3	2×2	0.2
GaAs	3.61-*j*0	4	2×2	0.2

Table 4.2: Shorted samples parameters

After running the simulation, an incident signal $E_{in}(t)$ (shown in Figure 4.6) was sent from a THz source placed at port 1 toward the sample. The ports 1 and 2 receives multiple reflections and transmissions caused by the propagation of the signals. Figure 4.7 and Figure 4.8 show the reflections for both the Si and GaAs samples, respectively.

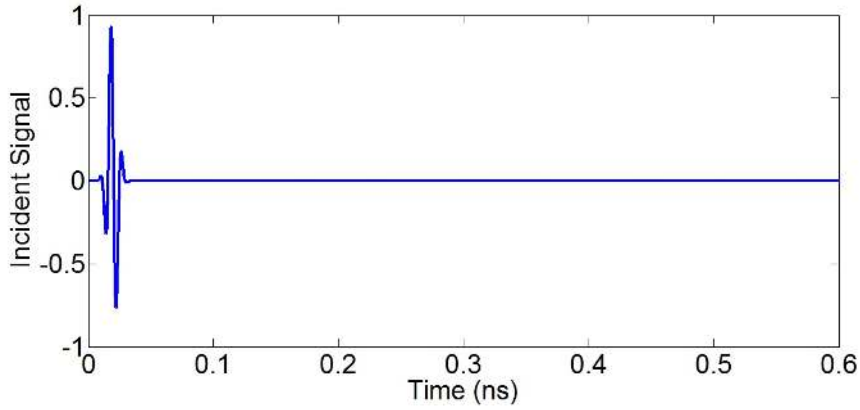

Figure 4.6: The THz incident signal

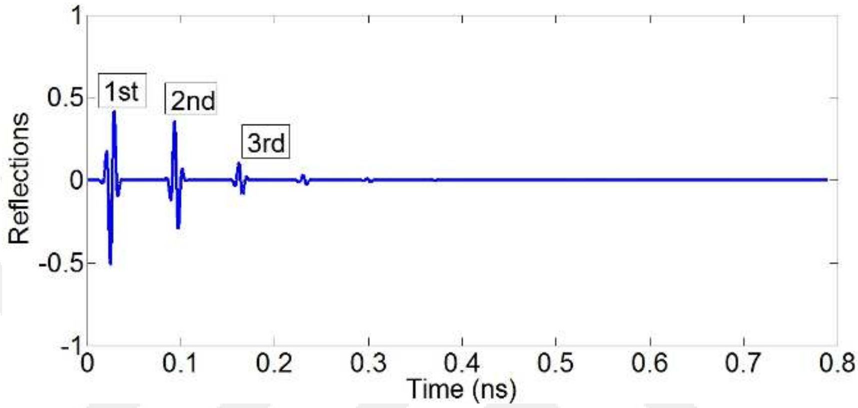

Figure 4.7: Reflection waves of the Si sample

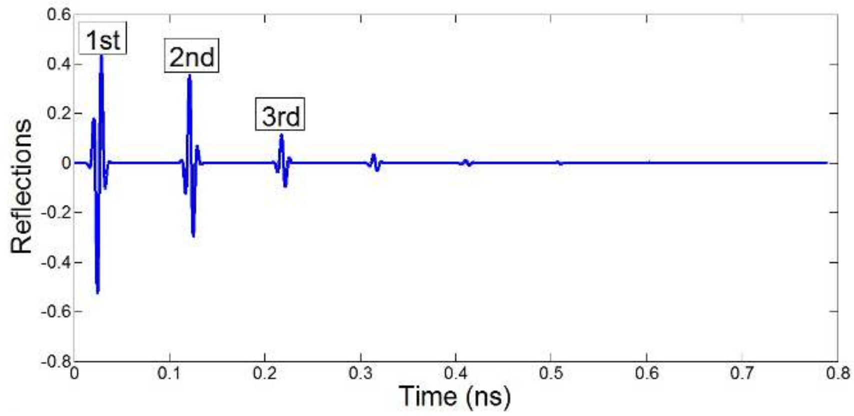

Figure 4.8: Reflection waves of the GaAs sample

From the Figures above we can see the first reflection $E_{r1}(t)$, second reflection $E_{r2}(t)$, and third reflection $E_{r3}(t)$. The sample thickness can be calculated using the equation from [20], which consider measuring the time of the first and second reflected waves arrivals at the *A* end. So the thickness can be calculated as the following

$$d = \frac{c(t_2 - t_1)}{2n_{real}}. \tag{4.1}$$

Where t_2 and t_1 are the times of the second and first reflected signal waves arrival and and n_{real} represents the real part of the studied sample. By taking the difference between two maximum values of the first and second reflections. The first maximum for the Si sample is t_1 = 0.029 ns and the second is t_2 = 0.0935 ns and by applying the equation we obtain d = 2.7 mm . For the GaAs sample t_1 = 0.029 ns and the second reflection is t_2 = 0.1214 ns so the sample thickness is d = 3.8 mm which are close values to the actual ones.
The transmission signals are shown in Figures 4.10 and 4.10 where E_{t1} represents the first transmission arrival at port 2, E_{t2} is the second transmission, and E_{t3} is the third transmission.

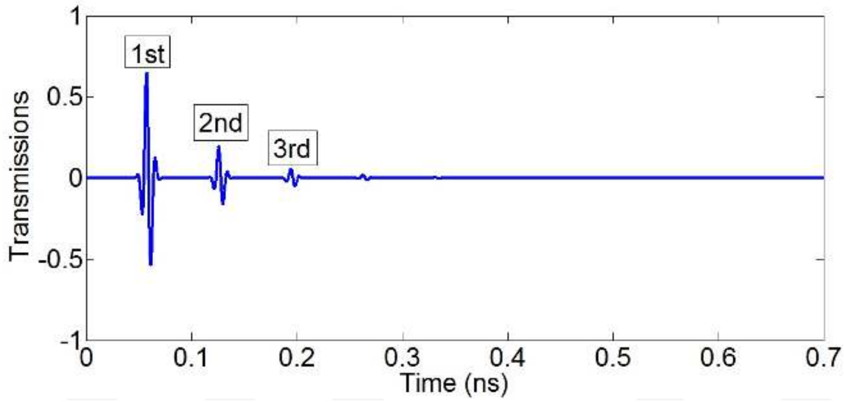

Figure 4.9: Transmission waves of the Si sample

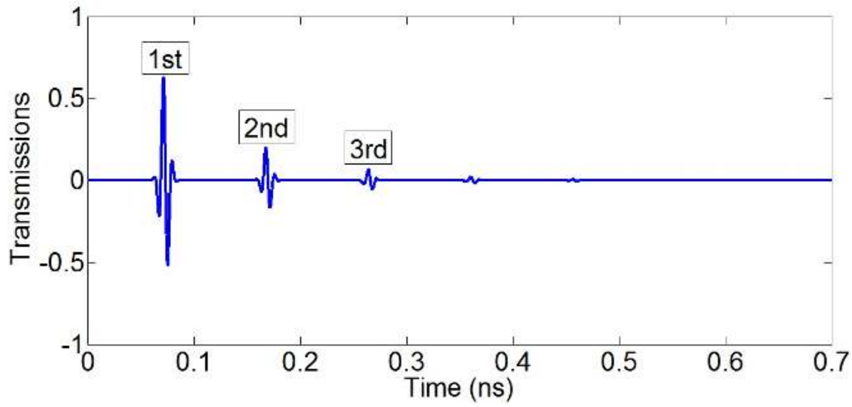

Figure 4.10: Transmission waves of the GaAs sample

The reflected waves for both Si and GaAs shorted samples are shown in Figure 4.11 and Figure 4.12. Following the same manner, To obtain the reflections of the shorted samples we followed the same steps, but as mentioned in the subsection 3.3.2 the existence of the PEC plate caused the transmission to be zero for both Si and GaAs samples. To calculate the sample thickness for the shorted sample we applied as previously the equation (4.1). So the first maximum for the Si sample is t_1 = 0.029 ns and the second is t_2 = 0.0975 ns aso the thicknedd is d = 2.8 mm . For the GaAs sample t_1 = 0.029 ns and the second reflection is t_2 = 0.1254 ns so the sample thickness is d = 3.99 mm.

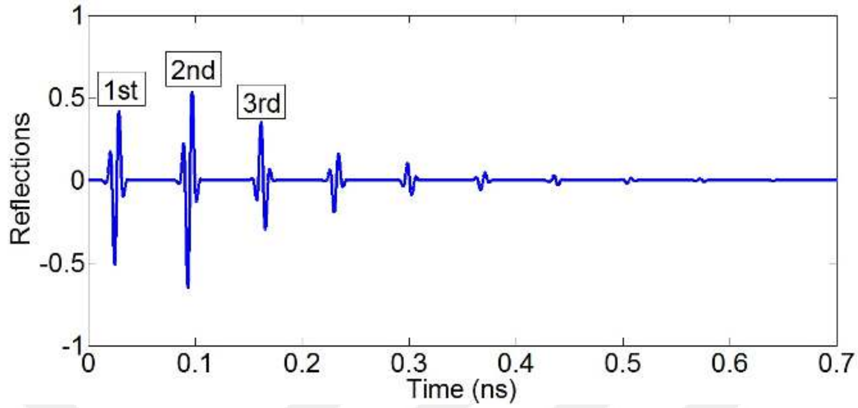

Figure 4.11: Reflection waves of the shorted Si sample

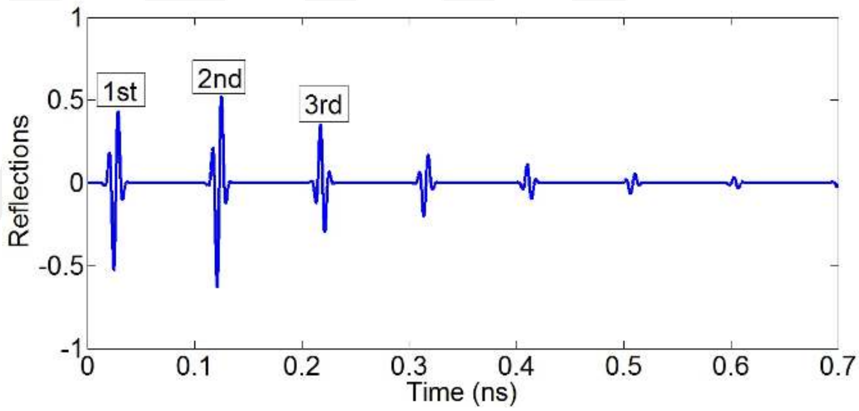

Figure 4.12: Reflection waves of the shorted GaAs sample

4.1.2 Application of time domain gating

To obtain the reflection and transmission signals separately, we applied a time gating at the desired portion of the signal by using the rectangular windowing [29], which is a simple gating technique to obtain the only desired portion of the signal. We selected a time period Δt_g for our desired portion of the signal and zeroed the remaining signal interval. We chose two different values of the time period in order to observe the effect of the time gating on our final results. The first value we considered is Δt_g = 0.023 ns and the second value is Δt_g = 0.059 ns. For the first gating period, the interval of the first reflection of the Si sample is $E_{r1}(t)$ = (0.0113-0.0343) ns, second reflection $E_{r2}(t)$

= (0.801-0.1031)ns, and third reflection $E_{r3}(t)$ = (0.1488-0.1718) ns. The Figures 4.13 to 4.15 show the chosen intervals selection for the Si sample.

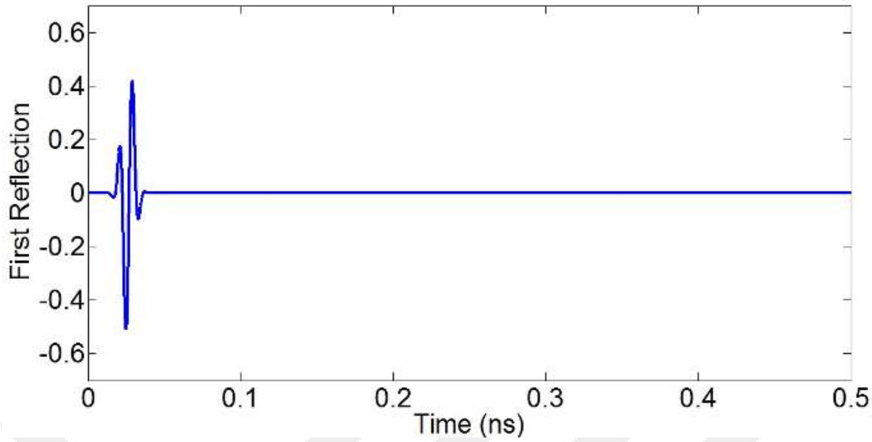

Figure 4.13: First gated reflection portion of the Si sample at Δt_g = 0.023 ns

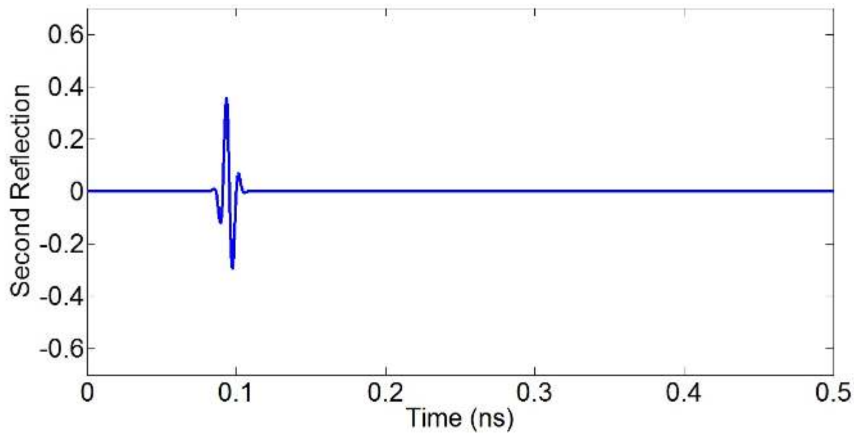

Figure 4.14: Second gated reflection portion of the Si sample at Δt_g = 0.023 ns

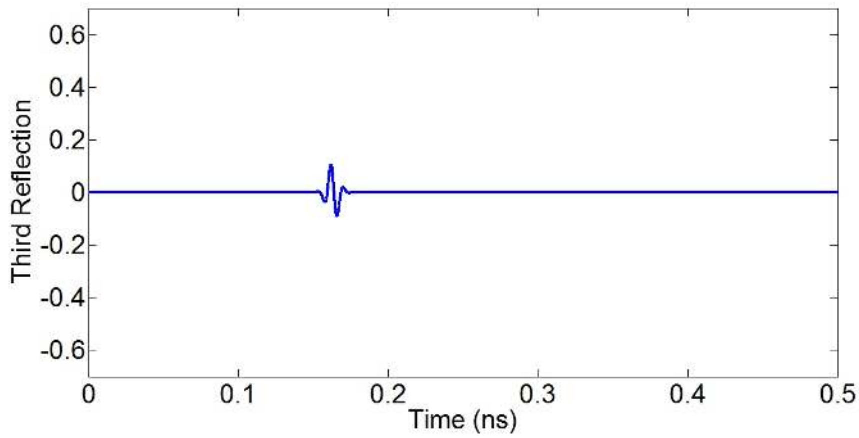

Figure 4.15: Third gated reflection portion of the Si sample at Δt_g = 0.023 ns

Similarly, the first gated transmission signal for the Si sample is $E_{t1}(t)$ = (0.0400-

0.063) ns and for the second $E_{t2}(t)$ = (0.1087-0.1317) ns, which are shown in Figures 4.16 and 4.17.

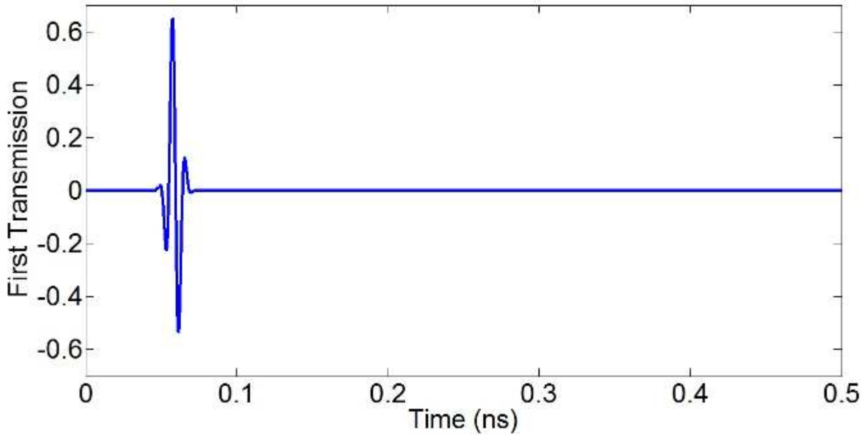

Figure 4.16: First gated transmission portion of the Si sample at Δt_g = 0.023 ns

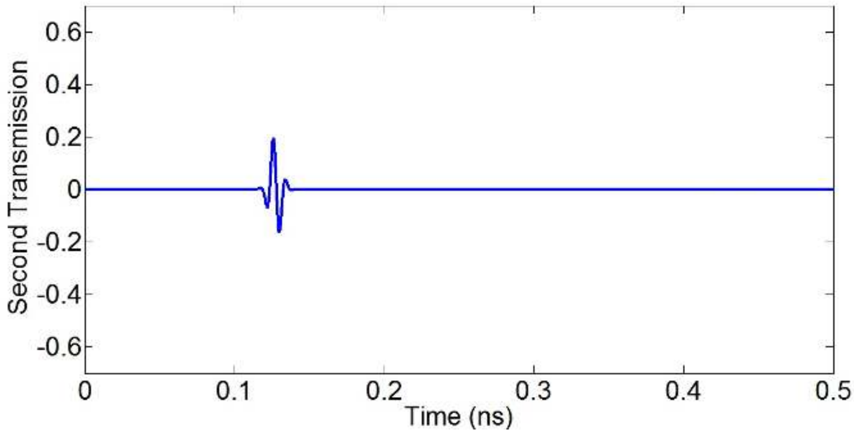

Figure 4.17: Second gated transmission portion of the Si sample at Δt_g = 0.023 ns

And the GaAs gated signals for the first three reflection are $E_{r1}(t)$= (0.0107-0.0337)ns for the first reflection, $E_{r2}(t)$ = (0.1084-0.1314)ns for the second reflection, and the third reflection $E_{r3}(t)$ = (0.2006-0.2236)ns as shown in Figures 4.18 to 4.20.

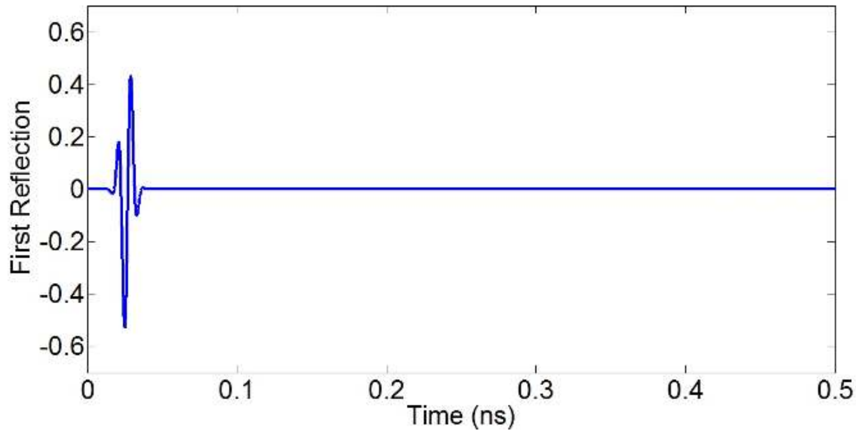

Figure 4.18: First gated reflection portion of the GaAs sample at Δt_g = 0.023 ns

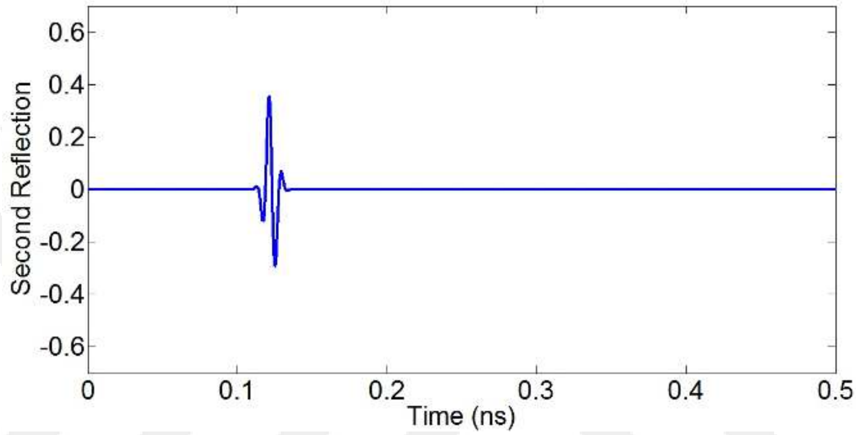

Figure 4.19: Second gated reflection portion of the GaAs sample at Δt_g = 0.023 ns

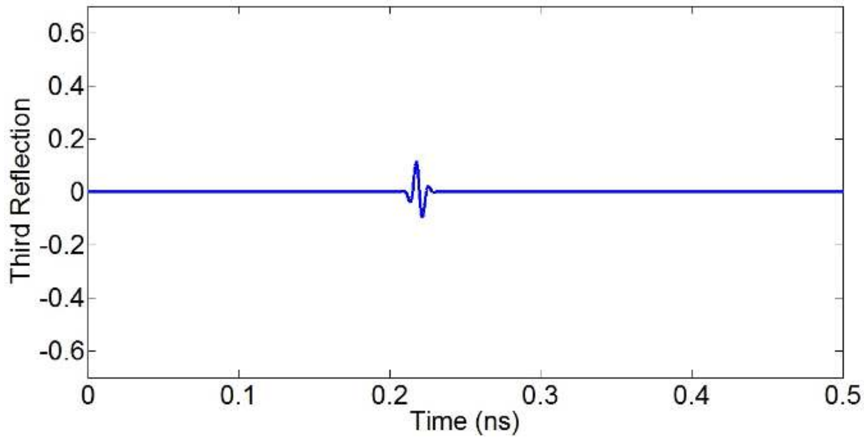

Figure 4.20: Third gated reflection portion of the GaAs sample at Δt_g = 0.023 ns

The gated transmission signals for GaAs sample are $E_{t1}(t)$ = (0.0562-0.0792) ns and for the second $E_{t2}(t)$ = (0.1540-0.177) ns, which are shown in Figures 4.21 and 4.22.

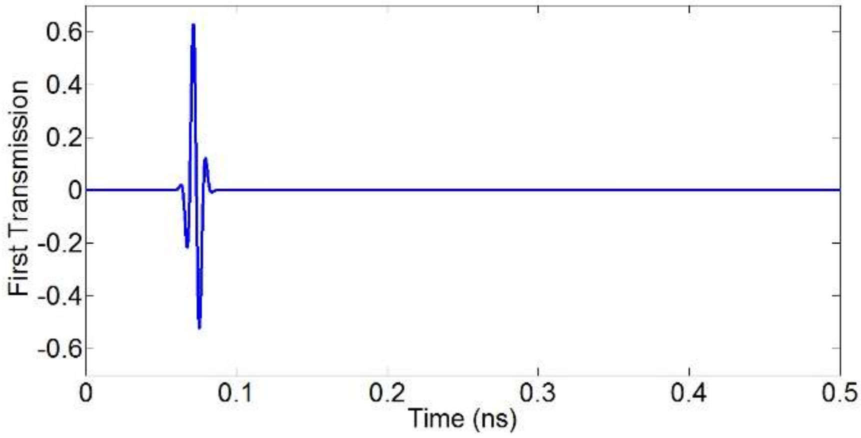

Figure 4.21: First gated transmission portion of the GaAs sample at Δt_g = 0.023 ns

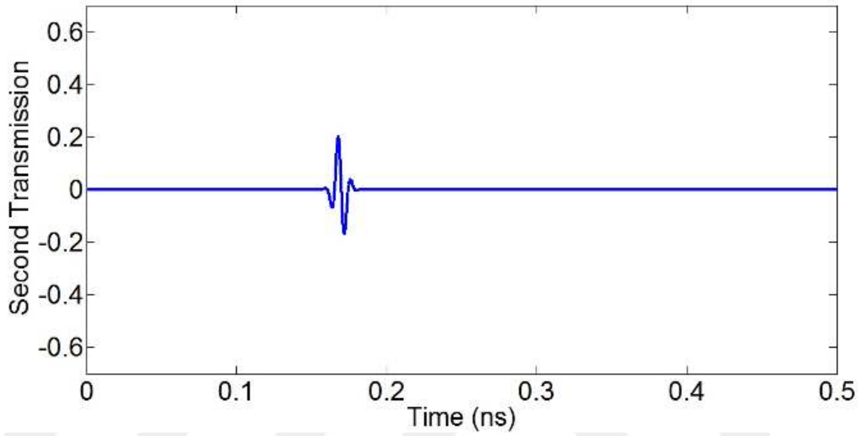

Figure 4.22: Second gated transmission portion of the GaAs sample at Δt_g = 0.023 ns

The gated signals for the shorted samples are obtained by the same steps we did with the normal samples. By taking Δt_g = 0.023 ns, the gated signals for shorted samples are depicted in the Figures 4.23 to 4.25 for the Si sample where the Si sample. So the first reflection is $E_{r1}(t)$= (0.0101-0.0331)ns, second reflection $E_{r2}(t)$= (0.0813-0.1043)ns, and third reflection $E_{r3}(t)$= (0.1474-0.1704)ns.

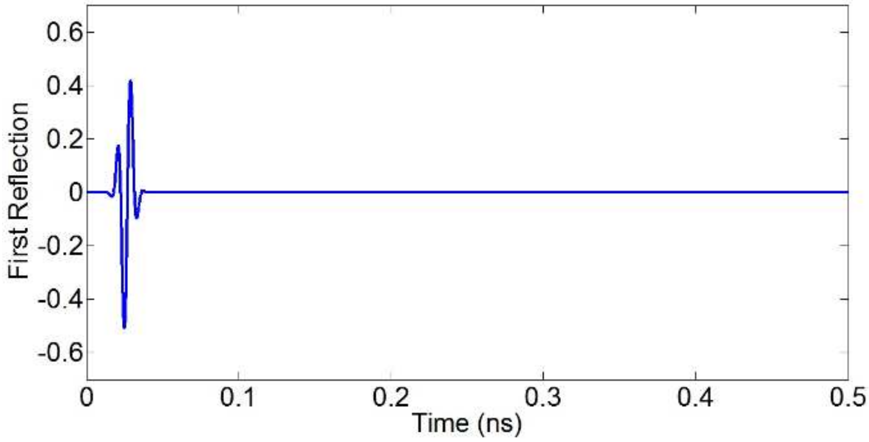

Figure 4.23: First gated reflection signal of the Si shorted sample at Δt_g = 0.023 ns

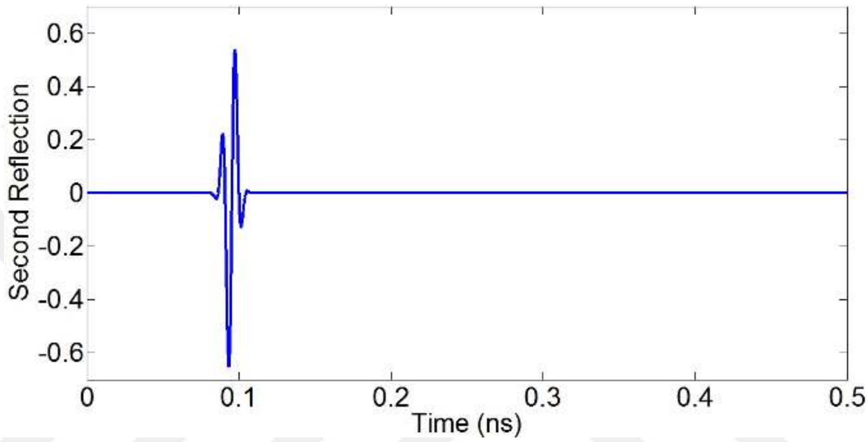

Figure 4.24: Second gated reflection signal of the Si shorted sample at Δt_g = 0.023 ns

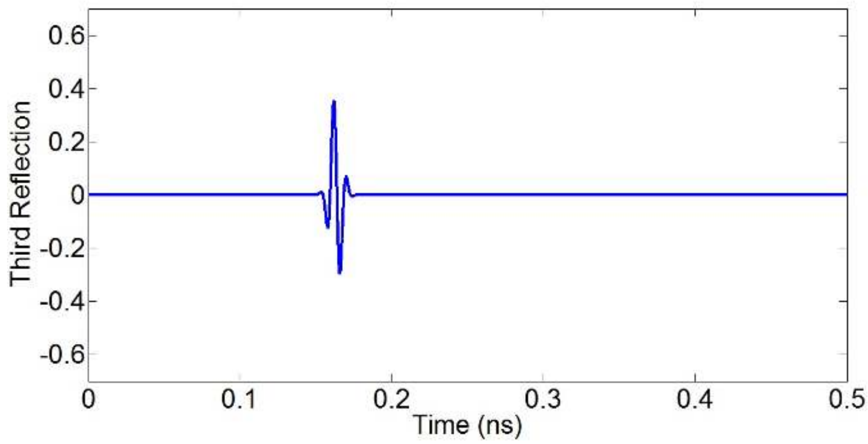

Figure 4.25: Third gated reflection signal of the Si shorted sample at Δt_g = 0.023 ns

For the shorted GaAs sample, the first reflection of the GaAs sample is $E_{r1}(t)$= (0.0098-0.0328)ns, second reflection $E_{r2}(t)$= (0.1089-0.1319)ns, and third reflection $E_{r3}(t)$= (0.2030-0.226)ns. Figures 4.26 to 4.28 show the gated GaAs shorted sample.

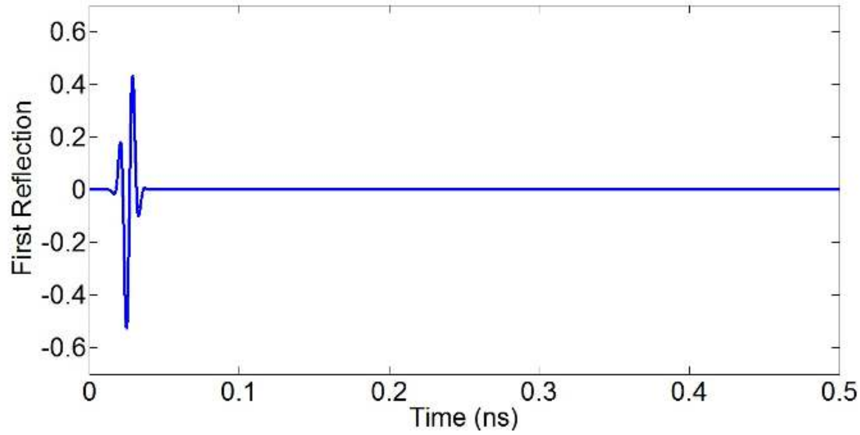

Figure 4.26: First gated reflection signal of the Si shorted sample at Δt_g = 0.023 ns

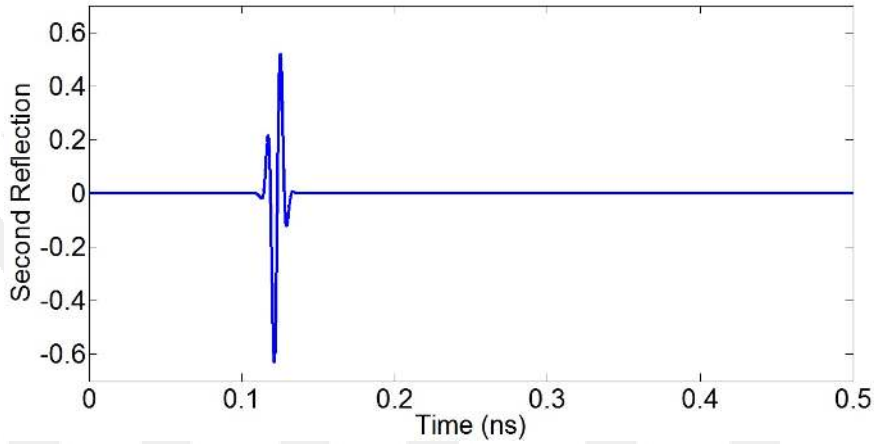

Figure 4.27: Second gated reflection signal of the Si shorted sample at Δt_g = 0.023 ns

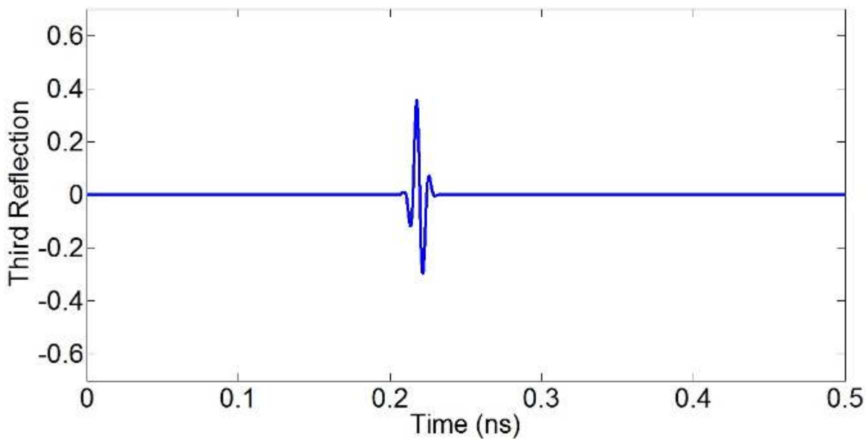

Figure 4.28: Third gated reflection signal of the Si shorted sample at Δt_g = 0.023 ns

For the second signal time gating Δt_g = 0.059 ns, the Si sample first reflection is given as $E_{r1}(t)$= (0.010-0.069)ns, second reflection $E_{r2}(t)$= (0.0686-0.1276)ns, and third reflection $E_{r3}(t)$= (0.1374-0.1964)ns. Figures 4.29 to 4.31 show the gating signals for the Si sample.

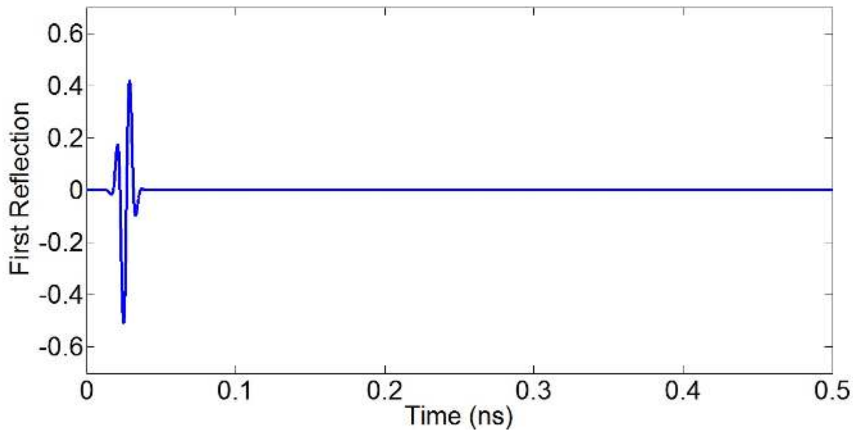

Figure 4.29: The first gated reflection of the Si sample at Δt_g = 0.059 ns

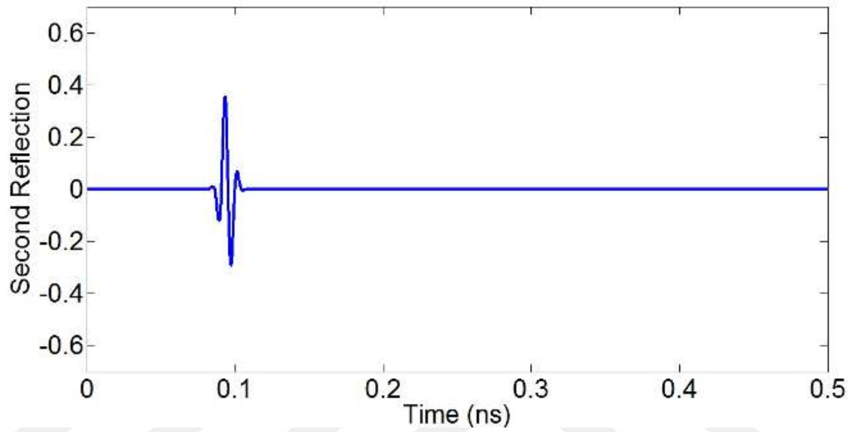

Figure 4.30: The second gated reflection of the Si sample at Δt_g = 0.059 ns

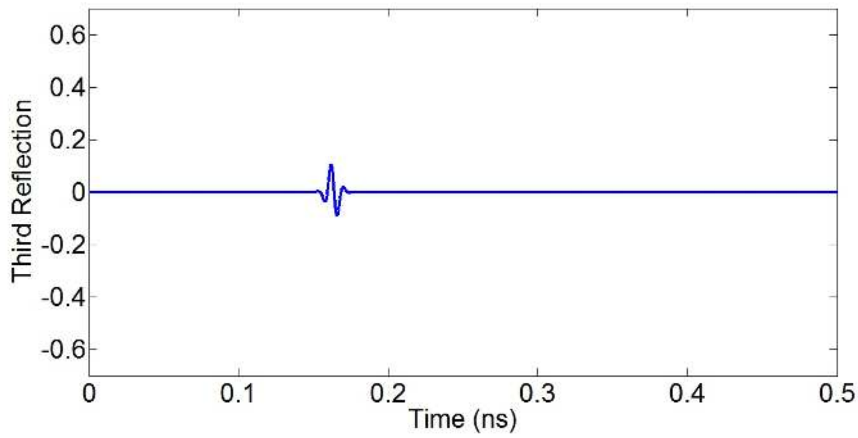

Figure 4.31: The third gated reflection of the Si sample at Δt_g = 0.059 ns

And for the gated transmission signals for Si with Δt_g = 0.059 ns, the gated portions are $E_{t1}(t)$= (0.0228-0.0818)ns, second transmission $E_{t2}(t)$= (0.0916-0.1506)ns and they are shown in Figures 4.32 and 4.33.

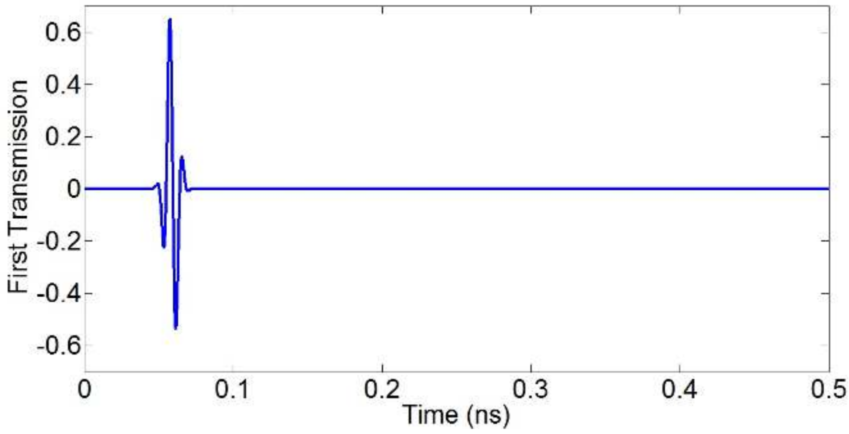

Figure 4.32: The first gated transmission of the Si sample at Δt_g = 0.059 ns

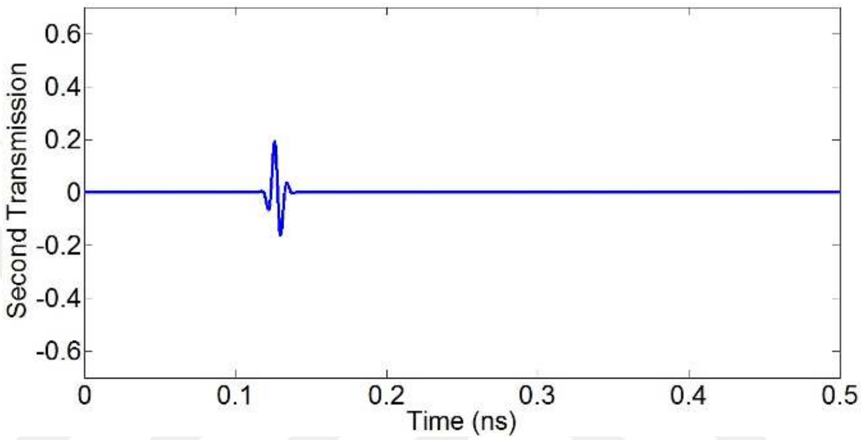

Figure 4.33: The second gated transmission of the Si sample at Δt_g = 0.059 ns

The GaAs sample first reflection at Δt_g = 0.059 ns is $E_{r1}(t)$= (0.0015-0.0605)ns, second reflection $E_{r2}(t)$= (0.0867-0.1457)ns, and third reflection $E_{r3}(t)$= (0.1952-0.2542)ns. Figures 4.34 to 4.36 show the gated signals for GaAs sample.

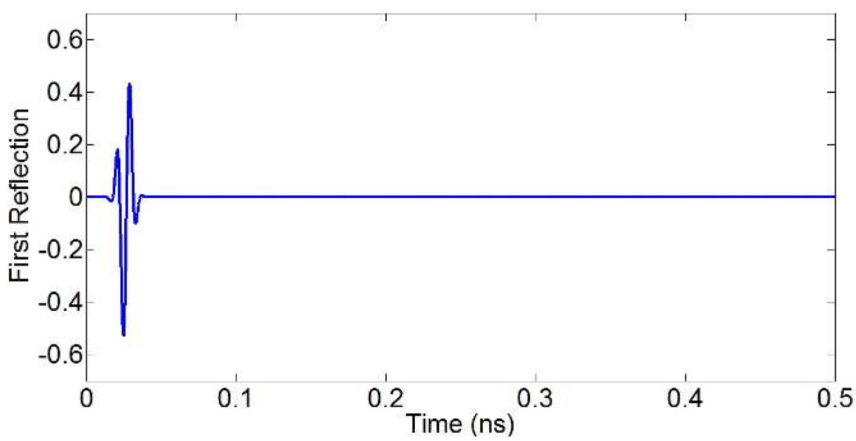

Figure 4.34: The first gated reflected signal of the GaAs sample for Δt_g = 0.059 ns

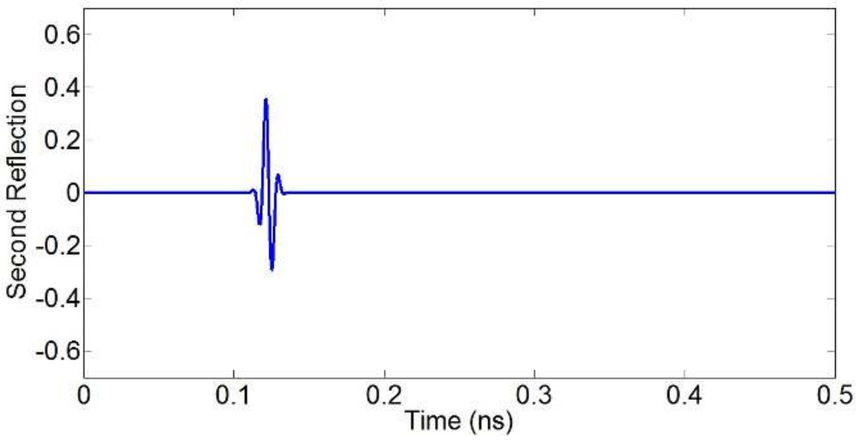

Figure 4.35: The second gated reflected signal of the GaAs sample for Δt_g = 0.059 ns

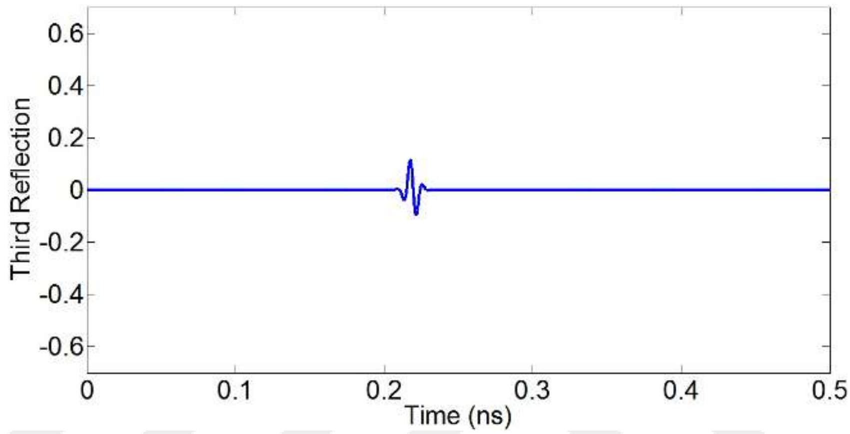

Figure 4.36: The third gated reflected signal of the GaAs sample for Δt_g = 0.059 ns

The gated Transmission signals for the GaAs sample for Δt_g = 0.059 ns are $E_{t1}(t)$= (0.0433-0.1023)ns for the first transmission and $E_{t2}(t)$= (0.1410-0.200)ns for the second transmission. Figures 4.37 and 4.38 shows these gated signals.

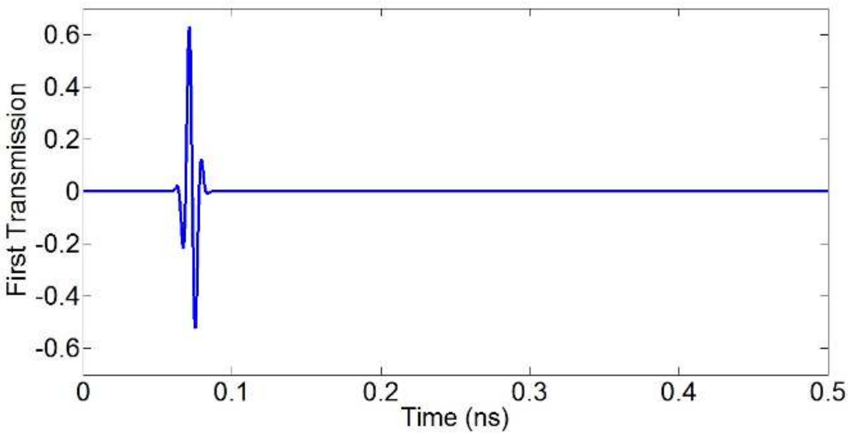

Figure 4.37: The first gated transmitted signal of the GaAs sample for Δt_g = 0.059 ns

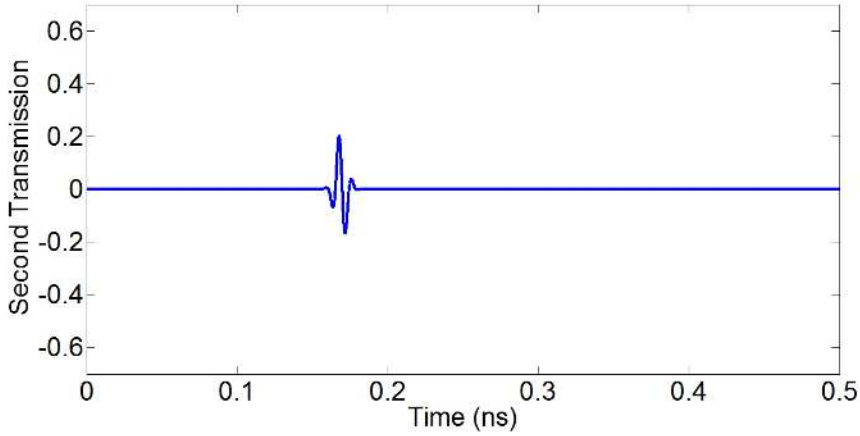

Figure 4.38: The second gated transmitted signal of the GaAs sample for Δt_g = 0.059 ns

In a same fashion, we obtained the gated signals for the shorted samples with Δt_g = 0.059 ns. So the first reflection of the Si shorted sample is $E_{r1}(t)$= (0.0050-0.064)ns, second reflection $E_{r2}(t)$= (0.0609-0.119)ns, and third reflection $E_{r3}(t)$= (0.1322-0.1912)ns and Figures 4.39 to 4.41 show the gating signals for shorted Si sample.

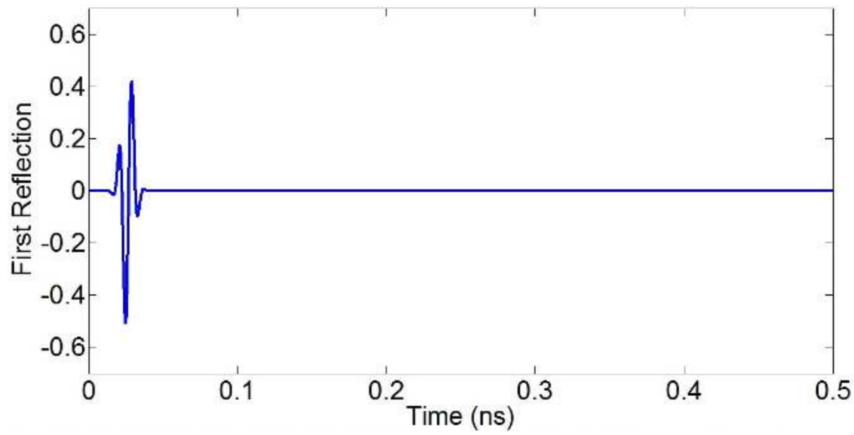

Figure 4.39: The first gated reflected signal of the Si shorted sample for Δt_g = 0.059 ns

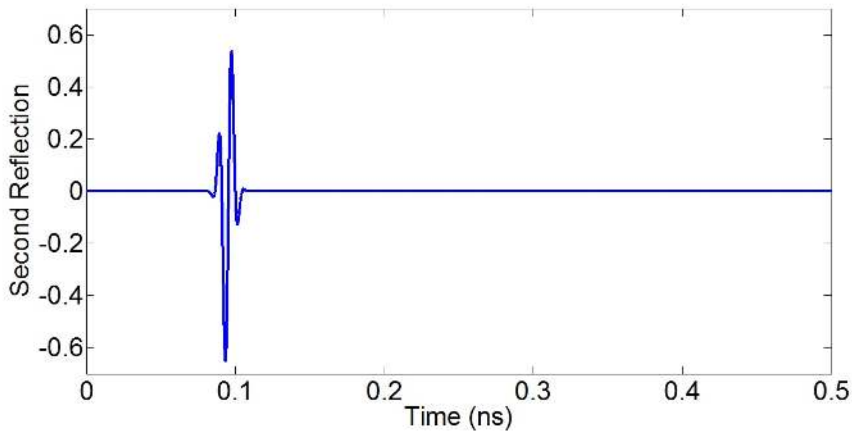

Figure 4.40: The second gated reflected signal of the Si shorted sample for Δt_g = 0.059 ns

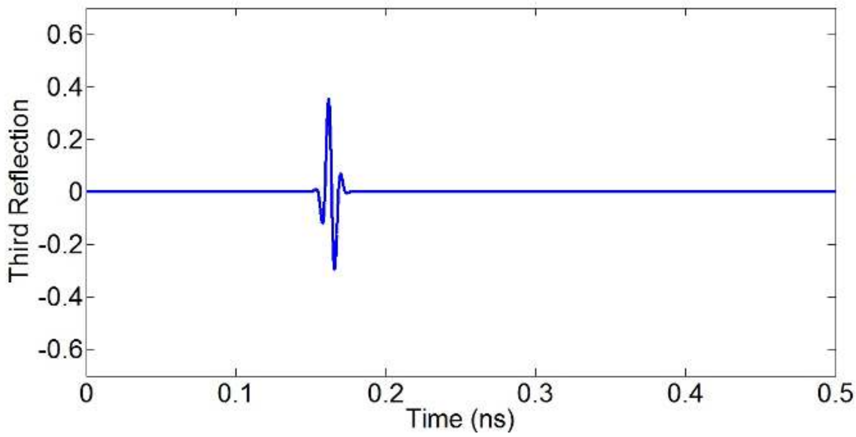

Figure 4.41: The third gated reflected signal of the Si shorted sample for Δt_g = 0.059 ns

For the GaAs sample first reflection is $E_{r1}(t)$= (0.0049-0.0639)ns, second reflection $E_{r2}(t)$= (0.0791-0.1381)ns, and third reflection $E_{r3}(t)$= (0.1881-0.2471)ns. Figures 4.42 to 4.44 show the gating signals for shorted GaAs sample.

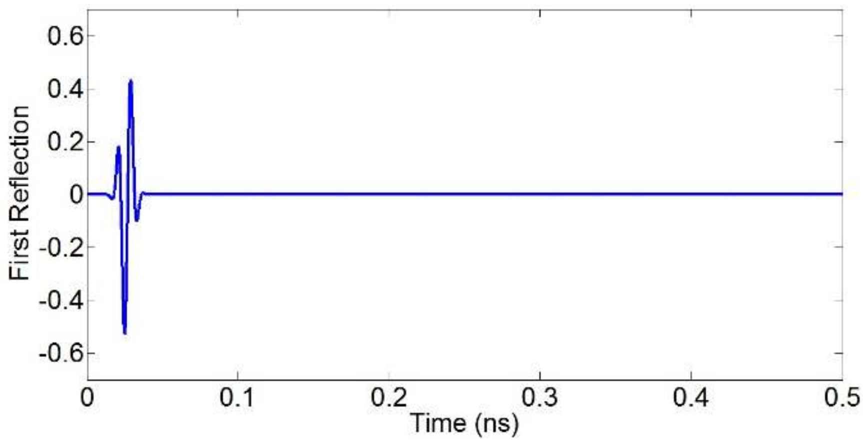

Figure 4.42: The first gated reflected signal of the GaAs shorted sample for Δt_g = 0.059 ns

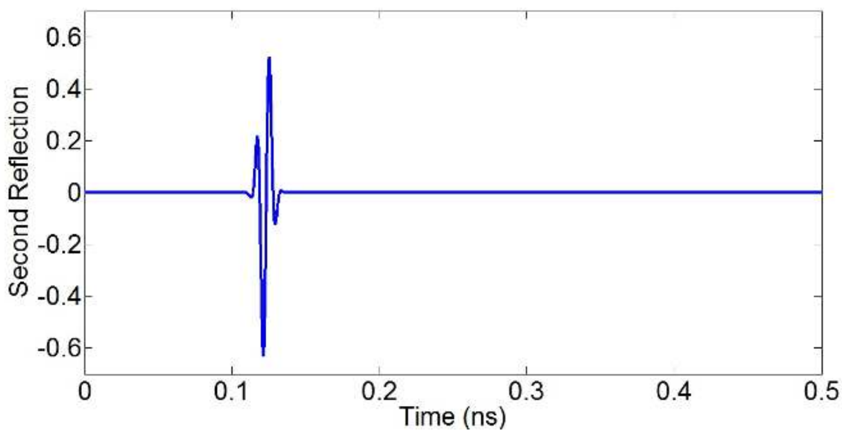

Figure 4.43: The second gated reflected signal of the GaAs shorted sample for Δt_g = 0.059 ns

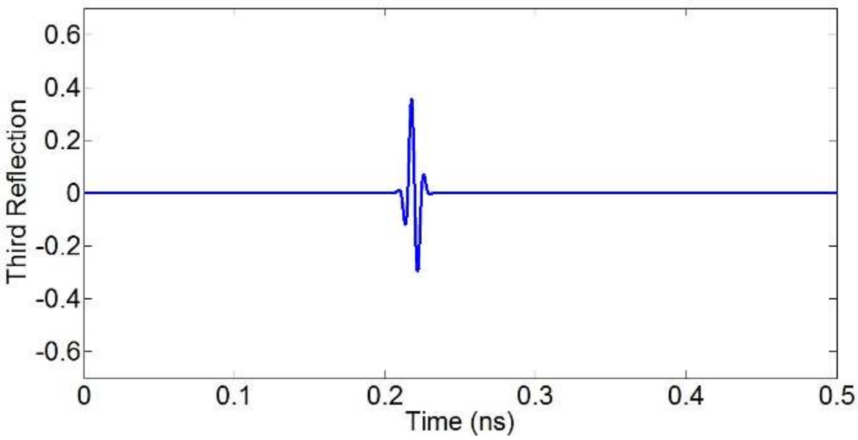

Figure 4.44: The third gated reflected signal of the GaAs shorted sample for Δt_g = 0.059 ns

4.1.3 The Frequency Domain Conversion

In the previous section we obtained the gated reflections of the samples in time-domain . In order to extract the optical parameters of the sample we must convert the gated time-domain signals into frequency-domain signals. We will do that by using the Fast Fourier Transform [30] which is given by the following formula.

$$F(k) = \sum_{n=0}^{N-1} a_n e^{-j2\pi \frac{k}{N}},$$

so

$$F(k) = \sum_{k=0}^{N/2-1} a_n^{even} e^{-j2\frac{K}{N/2}} + e^{-j2/N} \sum_{k=0}^{N/2-1} a_n^{odd} e^{-j2\frac{K}{N/2}}. \tag{4.2}$$

In equation (4.2) the $F(k)$ represents the number of samples and N is the number of computations. The FFT separate the even function of calculations a_n^{even} and the odd function of calculation of total function a_n^{odd} to simplify the total number of calculations required. We calaculate the FFT conversion using the MATLAB [31] function 'fft'. After the Matlab calculations we determined our frequency interval by taking the f_{sample}= 1/Δt_{CST} where the Δt_{CST} is provided from the CST simulation data, so the f_{sample}= (1/0.00010851278)ns $\approx$ 9215 GHz. The interval that we studied using the CST is lying between the (100-200) GHz, so in order to obtain the signal lying between these two frequencies we divide the sample frequency f_{sample} by the multiples of 2 until we reached the desired frequency. So by taking f_{sample}/32 $\approx$ 288 GHz and then we chose our studied intervals which lies between (100-200) GHz.

4.1.4 The Extraction of Optical Parameters

After chosing the frequency interval, we applied our method to extract the optical parameters. By using the equation (3.33) from previous chapter we obtained the optical parameters. We compared our method with the proposed method by Singh *et al.* [20]. The Figures 4.45 and 4.46 and show the refractive index real and imaginary parts of the Si sample correspondent to Δt_g = 0.023 ns.

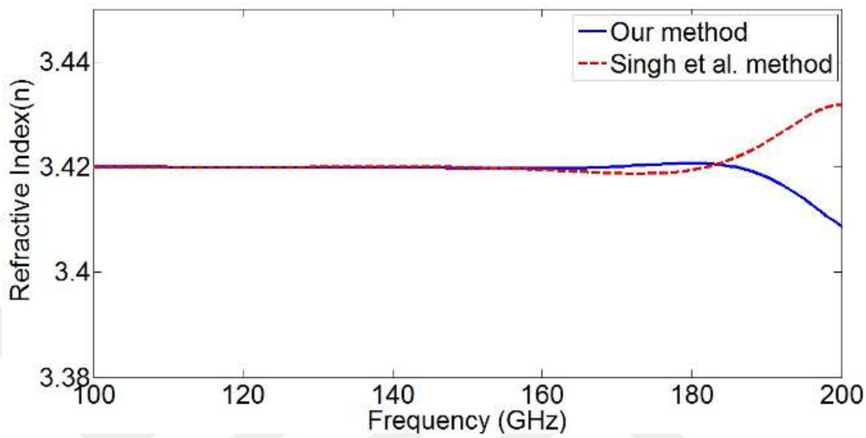

Figure 4.45: Real part of the Si sample for Δt_g = 0.023 ns

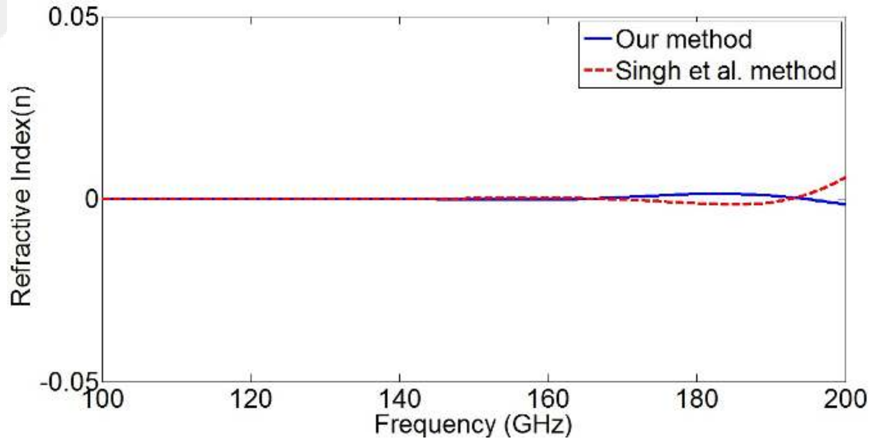

Figure 4.46: Imaginary part of the Si sample for Δt_g = 0.023 ns

The real and imaginary parts of the GaAs correspondent to Δt_g = 0.023 ns. sample are shown in Figures 4.47 and 4.48.

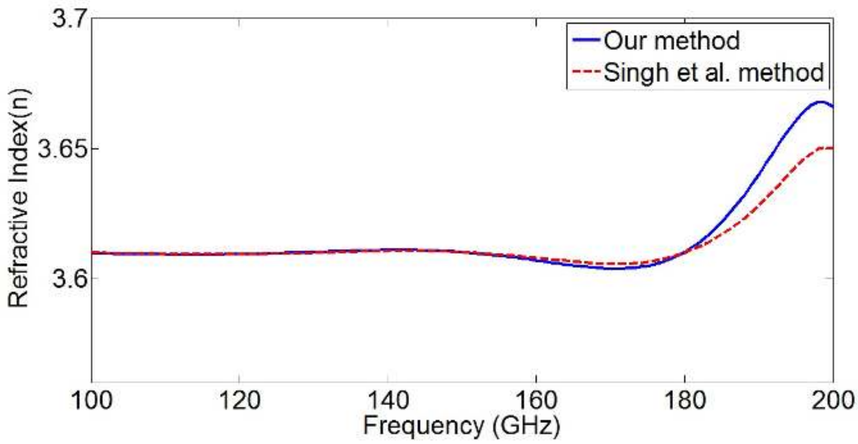

Figure 4.47: Real part of the GaAs sample for Δt_g = 0.023 ns

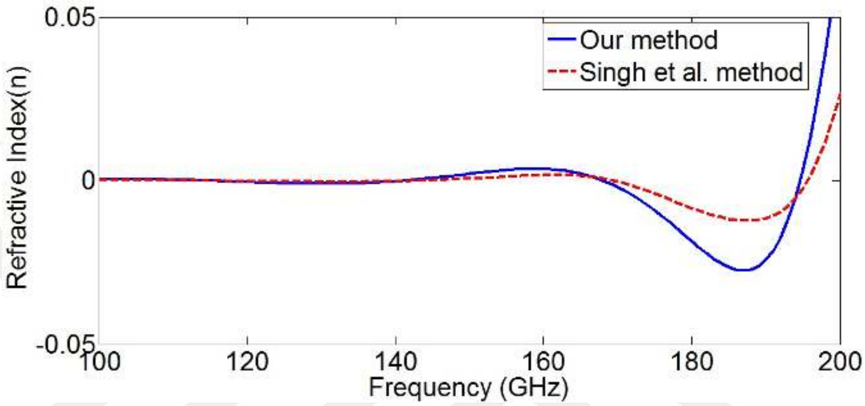

Figure 4.48: Imaginary part of the GaAs sample for Δt_g = 0.023 ns

The calculations was done the same with the shorted Si and GaAs samples . The Figures 4.49 and 4.52 show the refractive indices of the shorted Si sample correspondent to Δt_g = 0.023 ns.

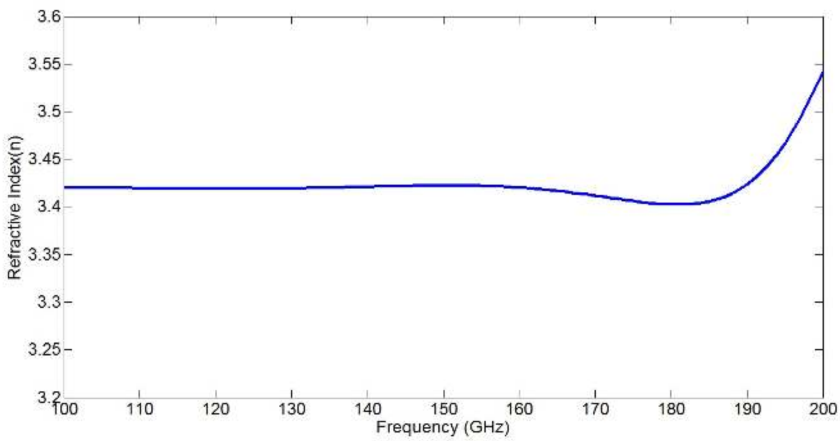

Figure 4.49: Real part of the Si shorted sample for Δt_g = 0.023 ns

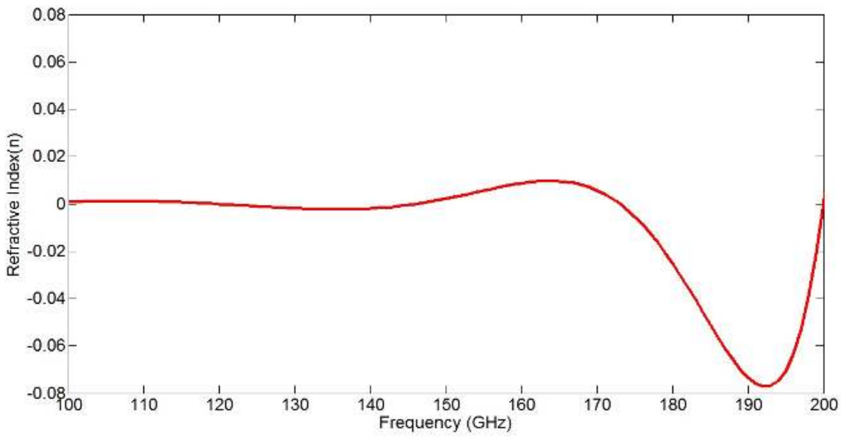

Figure 4.50: Imaginary part of the Si shorted sample for Δt_g = 0.023 ns

And same for real and imaginary parts for the shorted GaAs sample correspondent to Δt_g = 0.023 ns are shown in Figures 4.51 and 4.52.

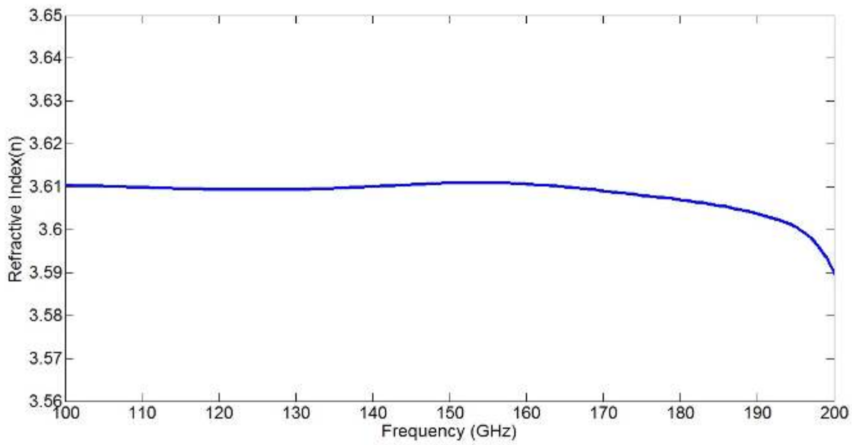

Figure 4.51: Real part of the GaAs shorted sample for Δt_g = 0.023 ns

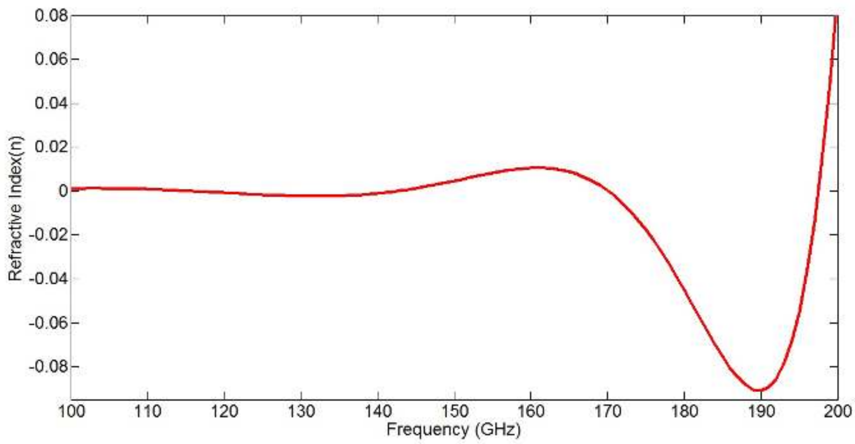

Figure 4.52: Imaginary part of the GaAs shorted sample for Δt_g = 0.023 ns

After that, we applied the optical parameters calculations according to the second gated signal value Δt_g = 0.059 ns. The real and imaginary parts related of the Si sample are shown in Figures 4.53 and 4.54 with comparison with the Singh *et al.* method.

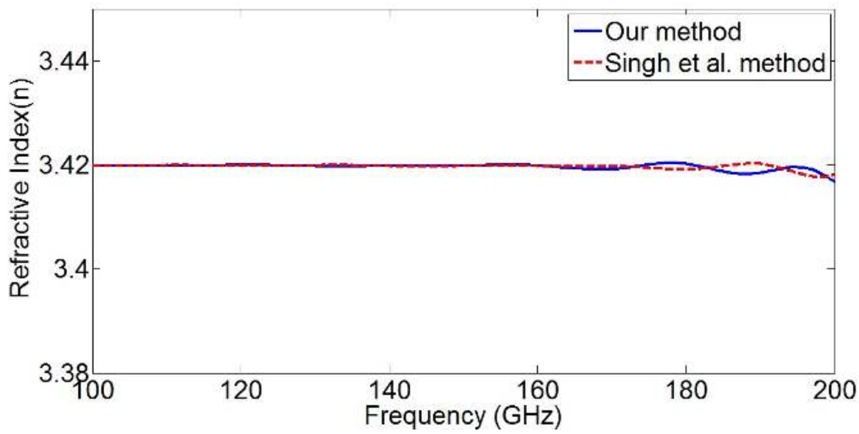

Figure 4.53: Real part of the Si sample for Δt_g = 0.059 ns

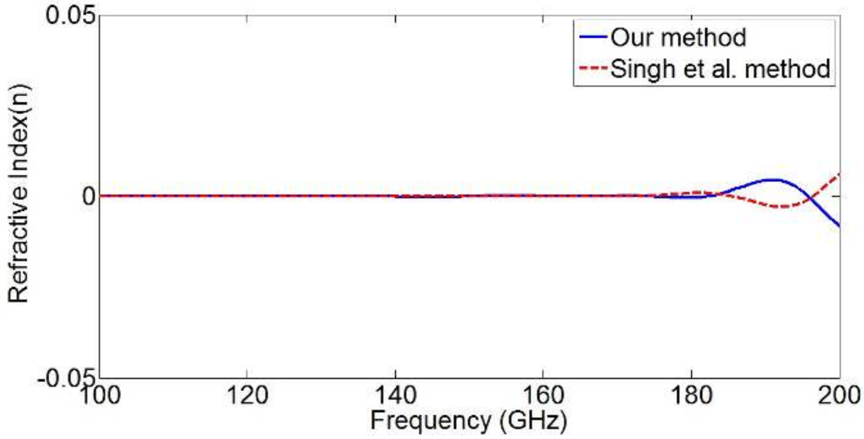

Figure 4.54: Imaginary part of the Si sample for Δt_g = 0.059 ns

The real and imaginary parts related to the GaAs sample of our method compared with Singh *et al.* correspondent to Δt_g = 0.059 ns are shown in Figures 4.55 and 4.56.

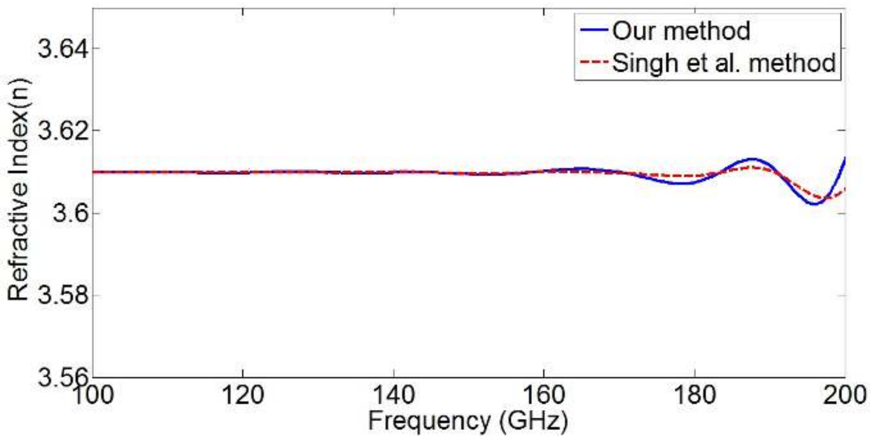

Figure 4.55: Real part of the GaAs sample for Δt_g = 0.059 ns

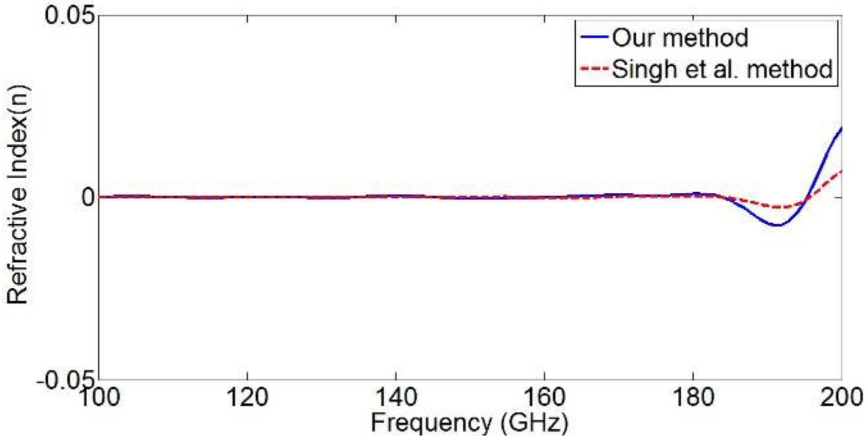

Figure 4.56: Imaginary part of the GaAs sample for Δt_g = 0.059 ns

With the same fashion, we obtain the real and imaginary parts for the shorted Si sample that correspondent to Δt_g = 0.059 ns which are shown in Figures 4.57 and 4.58.

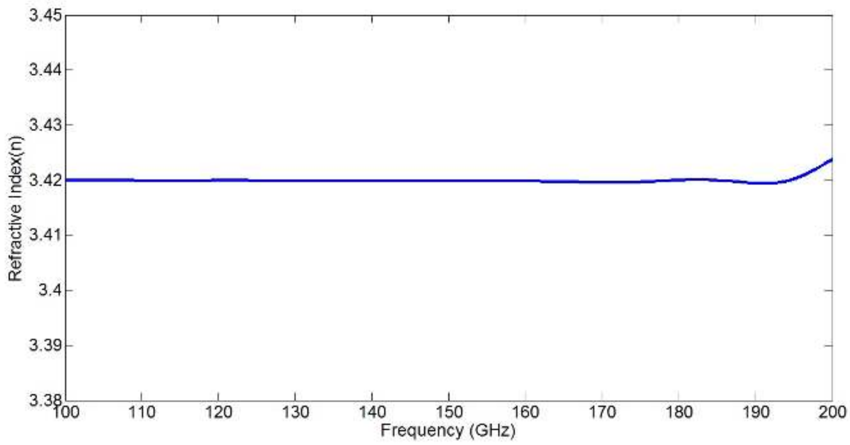

Figure 4.57: Real part of the Si shorted sample for Δt_g = 0.059 ns

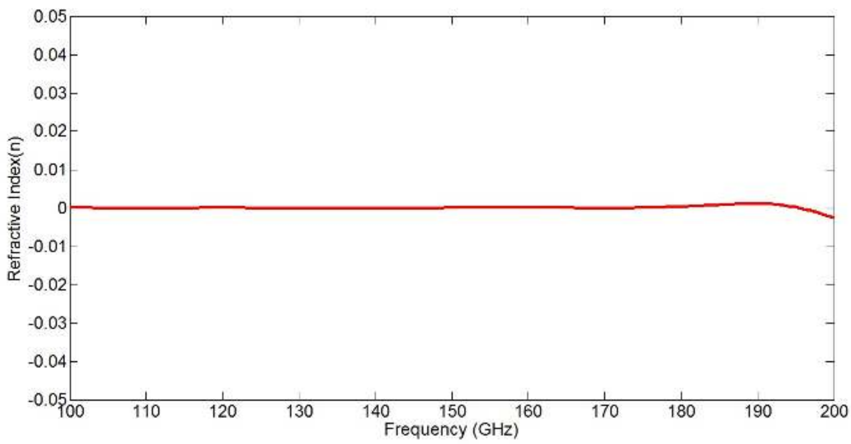

Figure 4.58: Imaginary part of the Si shorted sample for Δt_g = 0.059 ns

And the real and imaginary parts for the shorted GaAs sample that correspondent to Δt_g = 0.059 ns which are shown in Figures 4.59 and 4.60.

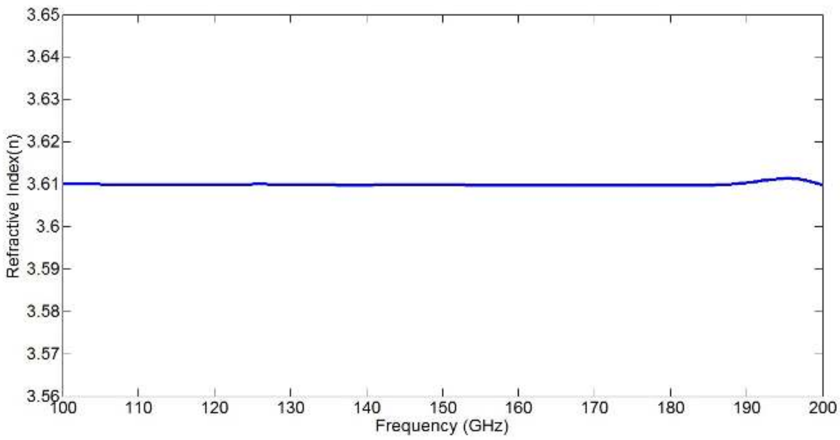

Figure 4.59: Real part of the GaAs shorted sample for Δt_g = 0.059 ns

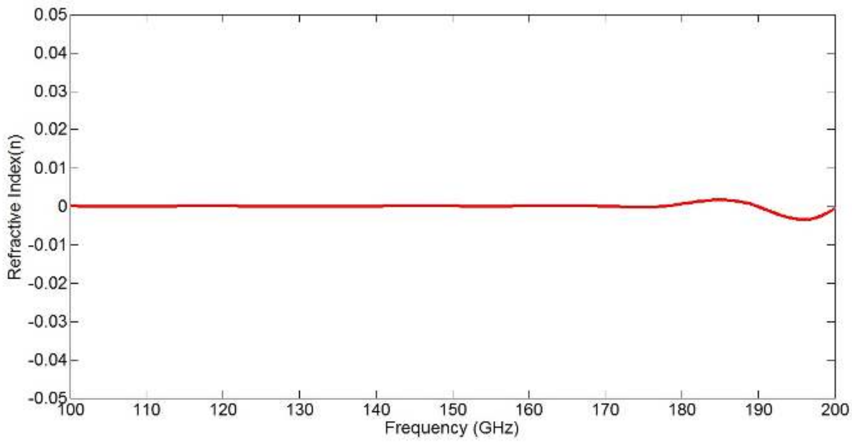

Figure 4.60: Imaginary part of the GaAs shorted sample for Δt_g = 0.059 ns

4.2 Error Analysis

After the calculation of the optical parameters and in order to evaluate the closeness of our results to the actual values, we used the standard deviation [32] for the error observation in our calculations. The formula to calculate the standard deviation is given as the following

$$\sigma = \sqrt{\frac{1}{n}\sum_{i=1}^{n}(x_i - x_m)^2}. \tag{4.3}$$

In the equation (4.3), x_i denotes the calculated refractive index with the proposed method, x_m is the actual refractive index (which in our case n_{sam}), and n is the total number of samples. For the calculations of the refractive index using the gating value $\Delta t_g = 0.023ns$ and after substituting in equation (4.3), the standard deviation values are given in Table 4.3 for the normal samples and in Table 4.4 for the shorted samples.

Sample	Refractive Index (n)	σ for real part	σ for imaginary part
Si	3.42-j0	0.0023	0.00057
GaAs	3.61-j0	0.0169	0.0139

Table 4.3: Standard deviation for the normal samples at $\Delta t_g = 0.023ns$

Sample	Refractive Index (n)	σ for real part	σ for imaginary part
Si	3.42-j0	0.0225	0.0263
GaAs	3.61-j0	0.0041	0.0327

Table 4.4: Standard deviation for the shorted samples at $\Delta t_g = 0.023ns$

And for the gating period $\Delta t_g = 0.059ns$, the standard deviation values are given in Table 4.5 for the normal samples and in Table 4.6 for the shorted samples.

Sample	Refractive Index (n)	σ for real part	σ for imaginary part
Si	3.42-j0	0.0006	0.0016
GaAs	3.61-j0	0.0019	0.0033

Table 4.5: Standard deviation for the normal samples at $\Delta t_g = 0.059ns$

Sample	Refractive Index (n)	σ for real part	σ for imaginary part
Si	3.42-j0	0.0001	0.0009
GaAs	3.61-j0	0.0003	0.0008

Table 4.6: Standard deviation for the shorted samples at $\Delta t_g = 0.059ns$

From these results we see that the selection of Δt_g can effect the accuracy of our method, and by that, the higher the value selected for gating the better the results we obtained. And on the other hand we can see that by adding the PEC plate we obtained better results of the optical material's parameters from the shorted samples compared with the normal samples. As we can see our proposed technique gave high accurate results compared with the actual values of the studied samples' refractive indices.

CHAPTER 5

CONCLUSION

In this work we introduced a novel THz time-domain spectroscopy technique to extract the material's optical parameters. In order to do that we used measurements of the first three reflection signals. By following our introduced formula in equation (3.31) we obtained the optical parameters values of the samples. Because of the usage of only the reflection geometry, we introduced another sample setup by placing a perfect electric conductor (PEC) in the back of the samples which blocked the transmittance between the sample and the *B* end. To validate our proposed technique, we used a full wave simulator called CST to study the behaviour of an electromagnetic wave in our theoretical configuration. We performed our test using two different samples which has two different refractive indexes (n_{sam}) and two different thickness values which are , Silicon (Si) sample and its refractive index is n_{Si}= 3.42 - *j*0 with a thickness of d = 3 mm and Gallium arsenide which has a refractive index of n_{GaAs}= 3.61 - *j*0 and a thickness of d = 4 mm. We used two different time gating $\Delta t_g = 0.023$ ns and $\Delta t_g = 0.059$ ns to invastigate the gating effects on the final parameters extraction results. We applied our method on both normal and shorted (PEC) backed geometries. We calculated the thickness of our samples by using the equation (4.1) from the provided CST data. After obtaining the gated time-domain signals we converted them into frequency domain signals in order to use our technique to extract the optical material's parameters and we compared it with the technique proposed in [20]. We tested the closeness of our results to the actual result by applying the standard deviation on both samples and both time gating values. Our technique showed a high accurate results compared with the actual refractive indexes values.

5.1 Potential Future Work

Our method gave an accurate results in lossless mediums. However, when the noise levels rises we won't be able to obtain a lot of reflections. Therefore, there will be a need to study extraction of the optical parameters within lossy medium environments. Another potential future work is to use our proposed method to study multi-layer structures.

REFERENCES

[1] Lee, Y.-S. (2009), Principles of terahertz science and technology, Springer,New York, NY.

[2] Pawar, A. Y. , Sonawane, D. D. , Erande, K. B. , Derle, D. V. (2013). Terahertz technology and its applications. *Drug invention today*, **5(2)**, 157-163.

[3] Ajito, K. (2015). Terahertz Spectroscopy for Pharmaceutical and Biomedical Applications, *IEEE Transactions on Terahertz Science and Technology*, **5(6)**, 1140 1145.

[4] Jackson,J. B. , Bowen,J. ,Walker, G. , Labaune,J. , Mourou,G. , Menu,M. , Fukunaga, K. (2011). A Survey of Terahertz Applications in Cultural Heritage Conservation Science, *IEEE Transactions on Terahertz Science and Technology*, **1(1)**, 220 231.

[5] Knipper, R., Brahm, A., Heinz, E., May, T., Notni, G., Meyer, H., Tnnermann, A., Popp, J. (2015). THz Absorption in Fabric and Its Impact on Body Scanning for Security Application,*IEEE Transactions on Terahertz Science and Technology* IEEE Transactions on Terahertz Science and Technology, **5(6)**, 999 1004.

[6] Sharma, V., Arya,D., Jhildiyal, M. (2011). Terahertz Technology and Its Applications , *5^{th} IEEE International Conference on Advanced Computing Communication Technologies*, Haryana, India.

[7] Shen, X., Dietlein, Ch. R., Grossman, E., Popovic, Z., Meyer, F. G. (2008). Detection and Segmentation of Concealed Objects in Terahertz Images,*IEEE Transactions on Image Processing*,**17(12)**, 2465 2475.

[8] van der Weide, D. W., Murakowski, J., Keilmann, F. (2000). Gas-Absorption Spectroscopy with Electronic Terahertz Techniques, *IEEE Transactions on Microwave Theory and Techniques* , **48(4)**, 740 743.

[9] Loh, J., Wang, Z., Thomson, M. J. (2016). Measuring Gas Temperature in Highly Particle Laden Flow Using Terahertz Spectroscopy, *IEEE Transactions on Terahertz Science and Technology*,**6(4)** , 518 524.

[10] Cherry, S. (2004). Edholm's law of bandwidth,*IEEE Spectrum* , **41(7)**, 58 60.

[11] Kim, S., Zajic, A. (2016). Statistical Modeling and Simulation of Short-Range Device-to-Device Communication Channels at Sub-THz Frequencies, *IEEE Transactions on Wireless Communications* , **15(9)**, 6423 6433.

[12] Naftaly, M. and Miles, R.E. (2007). Terahertz time-domain spectroscopy for material characterization. *Proceedings of the IEEE* , **95(8)**, 1658-1665.

[13] Mller, U., Cooke, D., Tanaka, K., Jepsen, P. (2009). Terahertz reflection spectroscopy of Debye relaxation in polar liquids [Invited], *J. Opt. Soc. Am. B*, **26(9)**, A113-A125.

[14] Zhong, H., Redo-Sanchez, A., Zhang, X. -C. (2006). Identification and classification of chemicals using terahertz reflective spectroscopic focal plane imaging system, *Opt. Express*, **14(20)**, 9130-9141.

[15] Duvillaret, L., Garet, F., and Coutaz, J. (1996). A Reliable Method for Extraction of Material Parameters in Terahertz Time-Domain Spectroscopy,*IEEE Journal of Selected Topics in Quantum Electronics* , **2(3)**, 739-746.

[16] Duvillaret, L., Garet, F., and Coutaz, J. (1999). Highly precise determinationof both optical constants and sample thickness in teraherz timedomain spectroscopy, *Appl Opt*, **38(2)**, 409-415.

[17] Dorney, T.D., Baraniuk, R.G., Mittleman, D.M. (2001). Material parameter estimation with terahertz time-domain spectroscopy,*J. Opt. Soc. Am.* , **18(7)**, 1562-1571.

[18] Pupeza, I., Wilk, R., Koch, M. (2007). Highly accurate optical material parameter determination with THz time-domain spectroscopy.*Optics express*, **15(7)**, 4335-4350.

[19] Hejase, J.A., Rothwell, E.J., Chahal, P. (2011). Self-calibrating technique for terahertz time-domain material parameter extraction, *J Opt Soc Am*, **28(12)**, 2561-2567 .

[20] Singh, S. P., Akhter, Z., Akhtar, M. J. (2015). Calibration independent estimation of optical constants using terahertz time-domain spectroscopy, *Microwave and Optical Technology Letters* , **57(8)**, 1861-1864.

[21] Huang, F., Federici, J.F., and Gary, D. (2004). Determining thickness independently from optical constants by use of ultrafast light,*Opt Lett* , **29(20)**, 2435-2437.

[22] Cheng, D.K.(1989). Field and wave electromagnetics, Pearson Education, India.

[23] Sogo, O., Oguchi, T. (2010). Electromagnetic wave propagation in rain and polarization effects, *Proceedings of the Japan Academy*, **86(6)**, 539-562.

[24] Balanis, C.A. (2012). Advanced engineering electromagnetics, 2^{nd} Edition , Wiley, Hoboken, NJ .

[25] Hasar, U.C., Barroso, J.J., Karacali, T., Ertugrul, M. (2015). Semi-infinite reflection coefficients of bi-anisotropic metamaterial slabs including boundary effects, *IEEE Microwave and Wireless Components Letters*, **25(5)**, 283-285.

[26] Hasar, U.C., Barroso, J.J., Bute, M., Muratoglu, A., Ertugrul, M. (2016). Boundary Effects on the Determination of Electromagnetic Properties of Bianisotropic Metamaterials From Scattering Parameters, *IEEE Transactions on Antennas and Propagation* , **64(8)**, 3459-3469.

[27] Losurdo, M. , Hingerl, K. (2013). Ellipsometry at the Nanoscale, Springer Science Business Media.

[28] CST-Computer Simulation Technology. (2014). Wellesley Hills, MA, Available at: http://www.cst.com.

[29] Boulanger, R., Lazzarini, V., Mathews, M. (2010). The audio programming book, MIT Press.

[30] Rao, K.R., Kim, D.N., Hwang, J.J. (2011). Fast Fourier transform Algorithms and Applications. Springer Science Business Media.

[31] Version, M. A. T. L. A. B. (2010). 7.10.0 (R2010a). The MathWorks Inc., Natick, MA.

[32] Holman, J.P., Gajda, W.J.(1994). Experimental methods for engineers (Vol. 2). New York, McGraw-Hill.

APPENDIX A

CURL TERM

The curl term is a spatial description of the non-uniform vector which can be described as the following :

$$\nabla \times g[x,y,z] = \begin{bmatrix} \vec{X} & \vec{Y} & \vec{Z} \\ \frac{\partial}{\partial x} & \frac{\partial}{\partial y} & \frac{\partial}{\partial z} \\ g_x & g_y & g_z \end{bmatrix} = \vec{X}(\frac{\partial g_z}{\partial y} - \frac{\partial g_y}{\partial z}) + \vec{Y}(\frac{\partial g_x}{\partial z} - \frac{\partial g_z}{\partial x}) + \vec{Z}(\frac{\partial g_y}{\partial x} - \frac{\partial g_x}{\partial y}) = vector$$

So the curl term is the cross product of the differential operator ∇.

APPENDIX B

WAVE PROPAGATION CONVENTIONS

In some scientific societies the convention of the wave propagation equation is given as the following :

$$E_i(\omega) = E_0 e^{\omega t - \vec{k}\vec{r}}$$

While others consider the following propagation convention :

$$E_i(\omega) = E_0 e^{\vec{k}\vec{r} - \omega t}$$

Where $\vec{k}$ is the wave vector and $\vec{r}$ is the direction of propagation.

APPENDIX C

THESIS RELATED PAPER

Optical Constant and Thickness Determination Using THz Time-Domain Reflection-Only Signals

Salah Haffar
and Ugur Cem Hasar
Electr. and Electron. Eng. Dept.
Gaziantep University
Gaziantep, 27310, Turkey
Email: uchasar@gantep.edu.tr

Joaquim Jose Barroso
Instituto Tecnológico de Aeronáutica
São José dos Campos 12242-680, SP, Brazil
E-mail: barroso@ita.br.

***Abstract*—A self-calibration noniterative technique for determination of the optical constants and thickness of lossless materials using only three reflection measurements is proposed. A generalized model is derived based on the reflection measurements. For validation, two different samples (Si and GaAs samples) are considered for extraction of their optical parameters and thicknesses by using a numerical full wave electromagnetic simulator. It is demonstrated that the proposed method can retrieve highly accurate results provided that reflected signal components are accurately separated.**

I. Introduction

The terahertz (THz) region is the electromagnetic spectrum lying between the microwave and infrared regions of the spectrum with a commonly used frequency range of 0.1-10 THz [1]. THz science and technology have immensely advanced as a consequence of recent improvements in ultrafast optoelectronics and low-dimensional semiconductor technologies [2]. The advantages of the THz frequency spectrum are that THz radiation has lower photonic energy, nonionizing nature, high water absorption properties and bandwidths [1] and good penetration into non-conducting and non-polar materials [2], [3]. Therefore, THz radiation has been applied in various areas such as pharmaceutical industry [4], biomedicine [5], security detections [6], gas sensing [7], and electromagnetic property extraction of coals [8].

THz spectroscopy techniques can grouped as a) reflection-type [9], [10] and b) transmission-type. While the reflection spectroscopy is applicable for absorbing materials, transmission spectroscopy gives the information about the whole of materials. In our current study, we will concentrate on THz spectroscopy techniques with transmission-mode. The THz techniques in the literature either need to send out a reference signal to self-calibrate the system or require precise knowledge of the sample thickness. It has been demonstrated in [11] that inaccurate knowledge of the sample thickness greatly influences the determination of optical constants. In order to determine the sample thickness, Duvillaret *et. al.* [11] proposed a numerical technique using the transfer function. It gives precise sample thickness values provided that an initial guess for the sample thickness is close to the real sample thickness value, which otherwise can yield to erroneous thickness evaluation due to the numerical method. Dourney *et. al.* [11] proposed a technique to estimate the sample thickness by using deconvolution. Since it is also a numerical technique, which is a time-consuming process, its accuracy can be reduced by an incorrect information of the sample thickness. In addition, their technique needs a reference measurement as the technique in [12] does. However, any inaccurate information of the reference signal could drastically alter the accuracy of thickness measurements. Besides, in order to remove the effect of inaccurate reference signal on extracted optical properties, Hajase *et. al.* [13] proposed a self-calibration process. Nonetheless, the accuracy of their approach decreases by inaccurate information of the sample thickness. Recently, Singh *et. al* [14] accomplished the non-iterative optical constant determination without using any reference signal. They determined the information of the thickness from a simple formula, which takes into account of travel time through the sample. However, they technique requires reflection and transmission measurements of four signals.

In this study, we propose another THz spectroscopy technique to non-iteratively determine optical properties of materials using reflection-only measurements of three signals. For validation, we extracted the optical constants of both the Gallium arsenide (GaAs) and Silicon (Si) samples with thicknesses of 4.0 mm. This method will overcome the need of the reference data and the sample thickness, and reduce the need for both transmitted and reflected signal analysis to only reflected signal analysis.

II. THEORETICAL STUDY

To derive the model, we consider the multiple reflection model in Figure 1. A THz source is placed at A, the distance between A and the sample is d_1, the thickness of the sample is d, and the distance between the sample and the B will be denoted as d_2. When the incident wave from the THz source impinge on the surface of the sample, some of the wave will be transmitted through the sample and some will be reflected at the sample (multiple reflections). The transmitted wave will undergo amplitude and phase variation while it travels through the sample. The material sample will have multiple

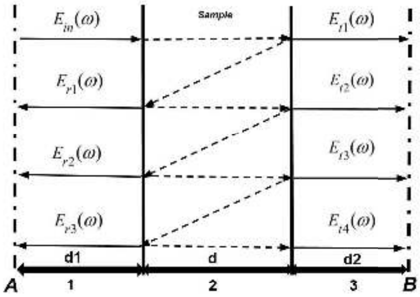

Fig. 1. Transmission and reflection waves representation in a homogenous medium

reflections of the incident waves caused by the Fabry-Perot [15] effect before exiting to the next end. Both the A and B ends will receive multiple signals caused by transmittance and reflectance and only five to six amplitudes which are above the noise level can be detected unambiguously.

In our theoretical analysis, we will consider only the reflected signals. Applying the ray-tracing method, the reflected signals can be expressed as

$$E_{r1}(\omega) = E_{in}(\omega) r_{12} R^2, \tag{1}$$

$$E_{r2}(\omega) = E_{in}(\omega) t_{12} r_{23} t_{21} T^2 R^2, \tag{2}$$

$$E_{r3}(\omega) = E_{in}(\omega) t_{12} r_{21} r_{23} r_{23} t_{21} T^4 R^2, \tag{3}$$

where

$$T = e^{-j\theta} \qquad \theta = (\omega) n_{\text{sam}} d/c,$$

and

$$R = e^{-j\theta_1} \qquad \theta_1 = (\omega) n_{\text{air}} d_1/c.$$

In the equations above, $E_{in}(\omega)$ is the amplitude of the incident electric field; r_{12}, r_{21}, and r_{23} represent, respectively, the reflection coefficients from region 1 to 2, from region 2 to 1, and from region 2 to 3; t_{12}, t_{21}, and t_{23} denote, respectively, the transmission coefficients through region 1 to 2, through region 2 to 1, and through region 2 to 3; c is the speed of light in free space; ω is the angular frequency; and n_{air} and n_{sam} are the complex refractive indices of air and the sample [15]. The Fresnel coefficients for both reflection and transmission for a normal incident wave is given as the following

$$r_{ij} = \frac{n_i - n_j}{n_i + n_j} \tag{4}$$

$$t_{ij} = \frac{2n_i}{n_i + n_j} \tag{5}$$

From (1)-(3) we obtain

$$\frac{E_{r2}^2(\omega)}{E_{r1}(\omega)E_{r3}(\omega)} = \frac{t_{12}t_{21}}{r_{12}r_{21}} \tag{6}$$

Substituting both (4) and (5) into (6) and assuming that n_i is n_{air} and n_j is n_{sam} yields

$$\frac{E_{r2}^2(\omega)}{E_{r1}(\omega)E_{r3}(\omega)} = \frac{4n_{\text{air}}n_{\text{sam}}}{(n_{\text{sam}} - n_{\text{air}})(n_{\text{air}} - n_{\text{sam}})}. \tag{7}$$

Assume that the complex refractive index of air equals to one $n_{\text{air}} = 1 - i0$ for simplicity, we obtain

$$\frac{4n_{\text{air}}n_{\text{sam}}}{(n_{\text{sam}} - n_{\text{air}})(n_{\text{air}} - n_{\text{sam}})} = M. \tag{8}$$

From (8), we obtain after some manipulation the following expression involving n_{sam} only

$$n_{\text{sam}}^2 M - n_{\text{sam}}(2M - 4) + M = 0. \tag{9}$$

By solving (9) we get

$$n_{\text{sam}} = \frac{(M-2) \mp \sqrt{(M-2)^2 - M^2}}{M}. \tag{10}$$

The correct sign for n_{sam} can be ascertained by applying the passivity condition; that is, $n_{\text{imag}} \leq 0$. Important feature of the expressions of n_{sam} in (10) is that n_{sam} can be non-iteratively and accurately determined without resorting to the information of the sample thickness d. In addition, when compared with the expression of the study in [14], n_{sam} can be computed by only using three reflection components instead of four signal components (two for transmission and two for reflection). By using this algorithm it can be possible to calculate the optical constant of a homogeneous medium without the need for transmission information or the need of reference measurements or pre-known sample thickness determination. One of the issues that must be taken into consideration is that this method will not be suitable if the noise levels are high so it is not suitable for materials considered as highly lossy mediums.

The sample thickness d can be calculated as in [14], by measuring the time difference of the first and second reflected signals reached to the A end as

$$d = \frac{c(t_2 - t_1)}{2n_{\text{real}}}, \tag{11}$$

where t_2 and t_1 are the time values corresponding to maximum of the second and first reflected signal components (see Fig. 5(a)).

III. RESULTS AND VALIDATION

To validate our proposed method we used a numerical three dimensional electromagnetic wave simulator, called Computer Simulation Technology Microwave Studio (CST-MWS) [16]. We build our sample geometry which is shown in Fig. 2 with geometrical details in Table I. By using the time domain solver provided by the simulator we obtained the transient analysis of the wave. The boundary conditions between port 1 and port 2 were applied by considering the perfect electric conductor in the a_x propagation direction and perfect magnetic conductor

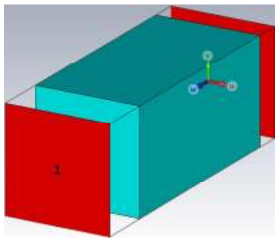

Fig. 2. The computational volume: the sample is asymmetrically positioned from the ports by distances $d_1 = 1$ mm and $d_2 = 0.5$ mm.

TABLE I
OPTICAL CONSTANT, THICKNESS, AND COMPUTATION AREA OF SI AND GAAS SAMPLES

Sample	Refractive index	Thickness (mm)	Area (mm $\times$ mm)
Si	$3.42 - i0.0$	2.0	2.0×2.0
GaAs	$3.61 - i0.0$	2.0	2.0×2.0

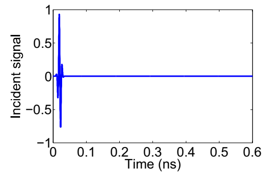

Fig. 3. The incident signal at THz frequency for both Si and GaAs samples.

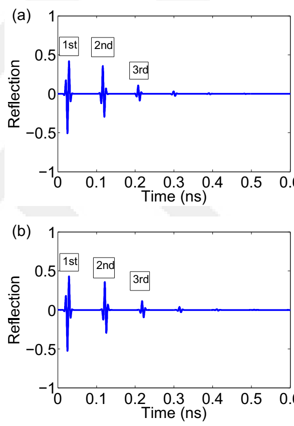

Fig. 4. Reflected signals of (a) the Si sample and (b) the GaAs sample.

in the a_y direction, and by opening the propagation in the a_z direction we ensure the plane wave radiation.

The both ports will receive multiple signals caused by transmitted and reflected multiple signals. We used the GaAs sample which has a refractive index of $3.61 - i0$ and Si sample which has a refractive index of $3.42 - i0$ as our testing samples. The thickness of both samples was chosen as $d = 4.0$ mm and area is set to 2×2 mm (see Fig. 2 and Table I). The procedure for obtaining the optical parameters is described as the following:

- Collect the reflection data provided by CST time domain simulator.
- Perform a time gating in order to take each individual signal separately.
- Apply the Fast Fourier Transform (FFT) to convert the gated time signals into the frequency domain.
- Use the proposed method to extract the optical parameters.

Figs. 3 and 4 show the time-domain incident and reflected signals for both Si and GaAs samples obtained for a frequency range of $100 - 200$ GHz. Although our proposed method does not require the incident signal (reference signal), we demonstrate it in Fig. 3 just for completeness. Upon applying the second step, it is important to determine the time range for gating (Δt_g). It should be selected in the manner that it includes as much signal portion (principal reflected component) as possible and it should not interfere with the region of other reflected signal portions. After analyzing the reflected signals in Figs. 4(a) and 4(b), we determined $\Delta t_g = 0.035$ ns for Si and then the time ranges of gating for the first reflected signal between $(0.010 - 0.045)$ ns, the second reflected signal $(0.100 - 0.135)$ ns, and the third reflected signal $(0.190 - 0.225)$ ns. The same gating procedure is repeated for GaAs sample by taking the first reflected signal between $(0.010 - 0.050)$ ns, the second reflected signal $(0.105 - 0.140)$ ns, and the third reflected signal $(0.205 - 0.235)$ ns. After taking the time-response of each individual signal, the rest of whole signal is zeroed to construct first, second, and third reflected signal components $E_{r1}(\omega)$, $E_{r2}(\omega)$, and $E_{r3}(\omega)$. Figs. 5(a)-5(c) illustrate the first, the second, and the third reflected signals from the Si sample obtained by zeroing the whole reflected signal except for the specific time range over which time-gating is obtained.

After obtaining the first, the second, and the third reflected signals for both Si and GaAs samples, we applied the 'fft' function of the MATLAB to compute the FFT transformed signals in frequency domain. Finally, we calculated n_{sam} from (10) by using the FFT transformed $E_{r1}(\omega)$, $E_{r2}(\omega)$, and $E_{r3}(\omega)$ for both samples. Figs. 6 and 7 show the real and imaginary parts of the extracted n_{sam} of Si and GaAs samples. It is seen from Figs. 6 and 7 that extracted n_{sam} values of both samples are in good agreement with their assumed values ($3.42 - i0$ for Si and $3.61 - i0$ for GaAs) as well as extracted values by the method in [14]. We note that extracted imaginary

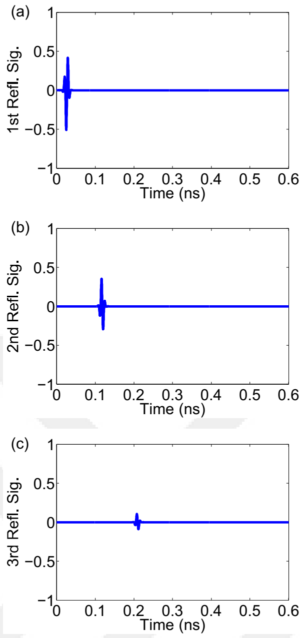

Fig. 5. (a) First, (b) second, and (c) third reflected signals the Si sample.

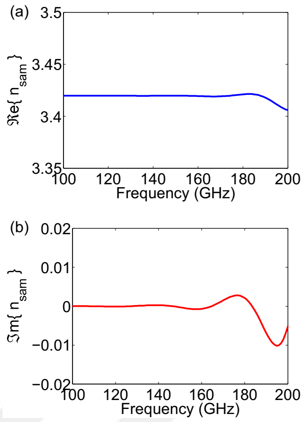

Fig. 6. Extracted (a) real and (b) imaginary parts of n_{sam} of the Si sample over 100-200 GHz.

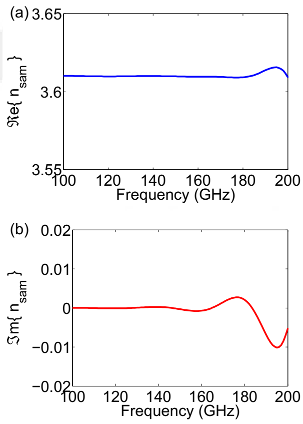

Fig. 7. Extracted (a) real and (b) imaginary parts of n_{sam} of the GaAs sample over 100-200 GHz.

part of n_{sam} is partly oscillating for both samples, which we think due to the selection of Δt_g. On the other hand, the sample thickness d was calculated from (11) by the time difference between maximum values of the first and second reflected signals. Calculated d values for GaAs and Si samples were around 4.2 mm and 4.1 mm, respectively. These values are very close to the assumed values 4.0 mm for both samples.

As noted in [14], our proposed method has two drawbacks. First, it requires the separation of the first, the second, and the third reflected signal components from the whole reflected signal for its application. Therefore, it is not suitable for extraction of optical constant and thickness of samples with small thicknesses. Second, it is not applicable for lossy samples since the levels of reflected signal components, especially the third one, will be drastically small.

IV. Conclusion

A novel technique for the optical constants and thickness determination of lossless samples by using THz time-domain signals. Our technique requires only three reflected signal components as compared to four signal components required by another technique in the literature. A generalized form is derived to obtain the optical parameters. An electromagnetic full wave simulator (CST-MWS) has been used for the validation. Optical constants and thicknesses of Si and GaAs are extracted by using our formalism for its validation.

Acknowledgment

The author, Ugur Cem Hasar, would like to thank the Scientific and Technological Council of Turkey (TUBITAK)

for supporting budget for the CST Microwave Studio.

REFERENCES

[1] Y. -S. Lee, *Principles of Terahertz Science and Technology*. Ney York: NY: Springer, 2009.
[2] T. Chang, X. Zhang, C. Yang, Z. Sun, and H. -L. Cui, 'Measurement of complex terahertz dielectric properties of polymers using an improved free-space technique,' *Meas. Sci. Technol.*, vol. 28, Art. ID. 045002, Feb. 2017.
[3] X. Zhang, T. Chang, H. -L. Cui, Z. Sun, C. Yang, X. Yang, L. Liu, and W. Fan "A free-space measurement technique of terahertz dielectric properties," *J. Infrared Milli. Terahz Waves*, vol. 38, no. 3, pp. 356-365, Mar. 2017.
[4] A. Y. Pawar, D. D. Sonawane, K. B. Erande, and D. V. Derle, "Terahertz technology and its applications," Drug Inv. Today, vol. 5, no. 2, pp. 157-163, Jun. 2013.
[5] K. Ajito, "Terahertz spectroscopy for pharmaceutical and biomedical applications," *IEEE Trans. THz Sci. Technol.*, vol. 5, no. 6, pp. 1140-1145, Nov. 2015.
[6] R. Knipper, A. Brahm, E. Heinz, T. May, G. Notni, H. G. Meyer, A. Tnnermann, and J. Popp, "THz absorption in fabric and its impact on body scanning for security application," *IEEE Trans. THz Sci. Technol.*, vol. 5, no. 6, pp. 999-1004, Nov. 2015.
[7] D. W. Van der Weide, J. Murakowski and F. Keilmann, "Gas-absorption spectroscopy with electronic terahertz techniques," *IEEE Trans. Microw. Theory Techn.*, vol. 48, no. 4, pp. 740-743, Apr. 2000.
[8] W. Fan, T. Chang, L. Liu, H. -L. Cui, "Dielectric properties of coal in the terahertz frequency region of 100500 GHz," *Fuel*, vol. 188, pp. 246-253, Jan. 2017.
[9] U. Mller, D. Cooke, K. Tanaka, and P. Jepsen, "Terahertz reflection spectroscopy of Debye relaxation in polar liquids [Invited]," *J. Opt. Soc. Am. B*, vol. 26, no.9, pp. A113-A125, 2009.
[10] H. Zhong, A. Redo-Sanchez, and X. -C. Zhang, "Identification and classification of chemicals using terahertz reflective spectroscopic focal plane imaging system," *Opt. Express*, vol. 14, no. 20, pp. 9130-9141, 2006.
[11] L. Duvillaret, F. Garet, and J. Coutaz, "Highly precise determination of both optical constants and sample thickness in teraherz timedomain spectroscopy," *Appl Opt*, vol. 38, no. 2,pp. 409415, 1999.
[12] F. Huang, J.F. Federici, and D. Gary, "Determining thickness independently from optical constants by use of ultrafast light," *Opt Lett* vol. 29,no. 20 ,pp. 24352437, 2004.
[13] J.A. Hejase, E.J. Rothwell, and P. Chahal," Self-calibrating technique for terahertz time-domain material parameter extraction," *J Opt Soc Am*,vol. A 28,no. , pp. 25612567 , 2011.
[14] S.P. Singh, Z. Akhter, and M. J. Akhtar, "Calibration independent estimation of optical constants using terahertz timedomain spectroscopy, " *Microwave and Optical Technology Letters*,vol.57, no. 8 ,pp. 1861-1864, 2015.
[15] C.A. Balanis, *"Advanced engineering electromagnetics,"* Hoboken: NJ :Wiley, 2012.
[16] CST-Computer Simulation Technology, Wellesley Hills, MA, 2014, Available at: http://www.cst.com.